

1 Fundamental Oxidation Processes in the Remote
2 Marine Atmosphere Investigated Using the NO-
3 NO₂-O₃ Photostationary State
4

5 Simone T. Andersen^{1*}, Beth S. Nelson¹, Katie A. Read^{1,2}, Shalini Punjabi^{1,2}, Luis Neves³,
6 Matthew J. Rowlinson¹, James Hopkins^{1,2}, Tomás Sherwen^{1,2}, Lisa K. Whalley^{2,4}, James D.
7 Lee^{1,2}, and Lucy J. Carpenter¹

8 ¹Wolfson Atmospheric Chemistry Laboratories (WACL), Department of Chemistry,
9 University of York, Heslington, York, YO10 5DD, UK.

10 ²National Centre for Atmospheric Science (NCAS), University of York, Heslington, York,
11 YO10 5DD, UK.

12 ³Instituto Nacional de Meteorologia e Geofísica, São Vicente (INMG), Mindelo, Cabo Verde.

13 ⁴School of Chemistry, University of Leeds, Leeds, LS2 9JT

14 *Corresponding author: simone.andersen@york.ac.uk

15

1 Abstract

The photostationary state (PSS) equilibrium between NO and NO₂ is reached within minutes in the atmosphere and can be described by the PSS parameter, ϕ . Deviations from expected values of ϕ have previously been used to infer missing oxidants in diverse locations, from highly polluted regions to the extremely clean conditions observed in the remote marine boundary layer (MBL), and have been interpreted as missing understanding of fundamental photochemistry. Here, contrary to these previous observations, we observe good agreement between PSS-derived NO₂ ($[\text{NO}_2]_{\text{PSS ext.}}$), calculated from measured NO, O₃, and $j\text{NO}_2$ and photochemical box model predictions of peroxy radicals (RO₂ and HO₂), and observed NO₂ ($[\text{NO}_2]_{\text{Obs.}}$) in extremely clean air containing low levels of CO (< 90 ppbV) and VOCs. However, in clean air containing small amounts of aged pollution (CO > 100 ppbV), we observed higher levels of NO₂ than inferred from the PSS, with $[\text{NO}_2]_{\text{Obs.}}/[\text{NO}_2]_{\text{PSS ext.}}$ of 1.12-1.68 (25th-75th percentile) implying underestimation of RO₂ radicals by 18.5-104 pptV. Potential NO₂ measurement artefacts have to be carefully considered when comparing PSS-derived NO₂ to observed NO₂, but we show that the NO₂ artefact required to explain the deviation would have to be ~ 4 times greater than the maximum calculated from known interferences. If the additional RO₂ radicals inferred from the PSS convert NO to NO₂ with a reaction rate equivalent to that of methyl peroxy radicals (CH₃O₂), then the calculated net ozone production rate (NOPR, ppbV/h) including these additional oxidants is similar to the average change in O₃ observed, within estimated uncertainties, once halogen oxide chemistry is accounted for. This implies that such additional peroxy radicals, cannot be excluded as a missing oxidant in clean marine air containing aged pollution, and that modelled RO₂ concentrations are significantly underestimated under these conditions.

2 Introduction

Tropospheric NO, NO₂ and O₃ are rapidly interconverted during the day via reactions (1-3), where NO is oxidised by O₃ into NO₂, which is then photolyzed into NO and O(³P), followed by a fast reaction of O(³P) with O₂ to return O₃.



47 The photostationary state (PSS) equilibrium between NO and NO₂ is reached within
 48 minutes (Leighton, 1961) if it is not impacted by fresh NO_x emissions and if the photolysis rate
 49 does not change quickly such as under rapidly changing cloud coverage (Mannschreck et al.,
 50 2004). The photostationary state can be described by the Leighton ratio (Leighton, 1961) (eq.
 51 I), where $j\text{NO}_2$ is the photolysis rate of NO₂ and ϕ is the PSS parameter.

$$52 \quad \phi = \frac{j\text{NO}_2[\text{NO}_2]}{k_1[\text{NO}][\text{O}_3]} \quad (\text{I})$$

53 Under conditions, where O₃ is the only oxidant converting NO to NO₂, such as during
 54 very low sunlight or very high NO mixing ratios ϕ is equal to 1 and NO₂ at PSS can be estimated
 55 from the measured NO, O₃, and $j\text{NO}_2$ (eq. II).

$$56 \quad [\text{NO}_2]_{\text{PSS}} = \frac{k_1[\text{NO}][\text{O}_3]}{j\text{NO}_2} \quad (\text{II})$$

57 Deviations from $\phi = 1$ suggest the presence of additional chemistry occurring (Calvert
 58 and Stockwell, 1983), particularly the conversion of NO to NO₂ by reaction with an oxidant
 59 other than O₃, such as hydroperoxy radicals (HO₂) and organic peroxy radicals (RO₂) (reactions
 60 4-5, where R represents any organic functional group) or with halogen oxides (IO, BrO;
 61 reactions 6-7) in the marine atmosphere.



66 By including these additional NO oxidation reactions, the NO₂ concentration at PSS
 67 can be estimated using equation (III). The photostationary state of NO/NO₂ can also be used to
 68 estimate the sum of HO₂ and RO₂ (RO_x) or the sum of BrO and IO (XO) in the atmosphere
 69 using equation (IV) and (V) and assuming that $k_4 = k_5$ and $k_6 = k_7$, respectively:

$$70 \quad [\text{NO}_2]_{\text{PSS ext.}} = \frac{(k_1[\text{O}_3] + k_4[\text{RO}_2] + k_5[\text{HO}_2] + k_6[\text{IO}] + k_7[\text{BrO}])[\text{NO}]}{j\text{NO}_2} \quad (\text{III})$$

$$71 \quad [\text{RO}_2] + [\text{HO}_2] = \frac{j\text{NO}_2[\text{NO}_2] - (k_1[\text{O}_3] + k_6[\text{IO}] + k_7[\text{BrO}])[\text{NO}]}{k_{4,5}[\text{NO}]} \quad (\text{IV})$$

$$72 \quad [\text{BrO}] + [\text{IO}] = \frac{j\text{NO}_2[\text{NO}_2] - (k_1[\text{O}_3] + k_4[\text{RO}_2] + k_5[\text{HO}_2])[\text{NO}]}{k_{6,7}[\text{NO}]} \quad (\text{V})$$

73 Previous studies reporting deviations in the PSS parameter to estimate RO_x
74 concentrations in the atmosphere are summarised in Table 1, which compares $[RO_x]_{PSS}$ against
75 measured and/or modelled $[RO_x]$. Measurements of RO_x are predominantly conducted using
76 chemical amplification, where each RO_2 and HO_2 molecule in ambient air leads to the
77 formation of several NO_2 molecules by chain reactions caused by the addition of high
78 concentrations of NO and CO (Cantrell et al., 1993b). The resultant NO_2 can be detected and
79 converted back to a RO_x concentration by quantification of the chain length of the reactions
80 via calibration, typically using known concentrations of CH_3O_2 or peroxyacetyl ($CH_3C(O)O_2$)
81 radicals (Cantrell et al., 1993b; Miyazaki et al., 2010; Wood and Charest, 2014). Since the basis
82 of the chemical amplification technique is detection of RO_x radicals from their ability to oxidise
83 NO to NO_2 (reactions 4 and 5), which is also used to estimate RO_x from the PSS, the RO_x
84 concentrations determined from these methods would be expected to agree reasonably well.
85 However, PSS-derived RO_x concentrations are generally higher than both measured values and
86 those calculated from models and steady state equations in rural conditions (Cantrell et al.,
87 1997; Cantrell et al., 1993a; Ma et al., 2017; Mannschreck et al., 2004; Volz-Thomas et al.,
88 2003) with exceptions such as in the Pearl River Delta where PSS-derived and measured RO_x
89 were comparable (Ma et al., 2017). During campaigns in relatively clean regions with moderate
90 influence from pollution (Amazon Basin and Arabian Peninsula), median PSS-derived
91 RO_x /modelled RO_x (both box and 3D) ratios have been shown to be around 1, albeit, with large
92 variations in the data (Tadic et al., 2020; Trebs et al., 2012). In the remote marine boundary
93 layer (MBL), PSS-derived RO_x has been observed to be 1.27 times higher than the measured
94 RO_x over the South Atlantic Ocean, which itself was approximately 4 times higher than box-
95 modelled (Hosaynali Beygi et al., 2011).

96 Differences between measured, modelled, and PSS-derived RO_x can be due to a variety
97 of reasons. RO_x concentrations calculated by box models rely on comprehensive constraint
98 from co-measured trace gases and a reaction scheme which accurately represents the most
99 important photochemical processes. Incomplete characterization of ambient trace gases and/or
100 reaction schemes can therefore result in uncertain RO_x predictions. Large deviations (factor of
101 ~ 3) between box modelled and measured RO_x levels in a pine forest in the Rocky Mountains
102 were attributed to a combination of a missing photolytic source of HO_2 at midday and a missing
103 reaction forming RO_2 independently of sunlight in the model scheme (Wolfe et al., 2014). PSS-
104 derived RO_x can be significantly over- or underestimated if PSS has not been established, for
105 example due to rapidly changing photolysis rates or local sources of NO_x (Mannschreck et al.,

106 2004). Another reason for overestimation of PSS-derived RO_x is NO₂ measurement artefacts
107 (Bradshaw et al., 1999; Crawford et al., 1996), which results in overestimated NO₂
108 concentrations. These are common in chemiluminescence instruments and can be due to
109 photolytic or thermal decomposition of HONO, peroxyacetyl nitrate (PAN), and other nitrate
110 molecules in the atmosphere (Bradshaw et al., 1999; Gao et al., 1994; Parrish et al., 1990;
111 Pollack et al., 2010; Reed et al., 2016; Ridley et al., 1988; Ryerson et al., 2000).

112 Measurements of RO_x are also not without challenges due to effects from e.g. the high
113 reactivity of RO_x, humidity, non-linearity of the NO₂ detection, and formation of organic
114 nitrates and nitrites. In the first chemical amplification instruments, NO₂ was detected by
115 luminol chemiluminescence, which has a non-linear response to NO₂ resulting in the need for
116 a multipoint calibration (Cantrell et al., 1997). However, more recent instruments use cavity
117 attenuated phase shift (CAPS) spectroscopy (Duncianu et al., 2020; Wood and Charest, 2014),
118 laser induced fluorescence (LIF) (Sadanaga et al., 2004), or cavity ring-down spectroscopy
119 (CRDS) (Liu and Zhang, 2014) for detection of NO₂, all of which have been shown to have a
120 linear response. Chemical amplifiers are usually only calibrated for one or two types of peroxy
121 radicals. However, the chain length of each peroxy radical varies, resulting in a different
122 amount of NO₂ production depending on the mixture of peroxy radicals present, which could
123 lead to over/underestimations depending on the ambient mixture. Additionally, the chain length
124 is significantly affected by humidity due to the increase in HO₂ wall loss on humid surfaces
125 and to an enhanced termination rate of HO₂ by reaction with NO to give HNO₃. HO₂ has been
126 shown to form a complex with H₂O (HO₂·H₂O), which reacts 4-8 times faster with NO, creating
127 HNO₃, at 50% relative humidity (RH) compared to under dry conditions (Butkovskaya et al.,
128 2007; Butkovskaya et al., 2009; Duncianu et al., 2020). This leads to the measured chain length
129 decreasing by a factor of two when going from dry conditions to 40% RH and by a factor of
130 three at 70% RH (Duncianu et al., 2020; Mihele and Hastie, 1998). Finally, the chain length is
131 impacted by the gas reagents (NO and CO). Peroxy radicals and alkoxy radicals (RO) can react
132 with NO to create organic nitrates and nitrites, which terminates the chain reaction, preventing
133 further radical propagation processes. This is favoured by longer chain peroxy radicals, and at
134 high NO concentrations. The formation yield of organic nitrates and nitrites differs from a few
135 percent to up to ~23% depending on the nature of the R group present (Duncianu et al., 2020).
136 The studies summarised in Table 1 using chemical amplification to measure total RO_x have
137 estimated the total uncertainty of the measurements to vary from 10-60% (1σ) with the most
138 recent study estimating the highest uncertainty (Ma et al., 2017).

139 In the presence of sufficient levels of NO, additional ambient peroxy radicals not
140 accounted for in photochemical models should lead to an underestimation of the simulated
141 production rate of O₃, which occurs via reactions (4) and (5) followed by photolysis of NO₂.
142 The production rate of O₃ (P(O₃)) can be calculated using equation (VI):

$$143 \quad P(\text{O}_3) = k_4[\text{NO}][\text{RO}_2] + k_5[\text{NO}][\text{HO}_2] \quad (\text{VI})$$

144 Volz-Thomas et al. (2003) calculated O₃ production rates from PSS-derived and
145 chemical amplification-measured RO_x during the BERLIOZ campaign in Pabstthum,
146 Germany, resulting in an average of ~ 20 ppbV h⁻¹ and ~ 2 ppbV h⁻¹ across the campaign,
147 respectively. The large difference was credited to an unknown process that converts NO into
148 NO₂ without causing additional O₃ production (Volz-Thomas et al., 2003). This is possible if
149 NO is oxidised by an oxidant which also destroys O₃, similarly to halogen atoms/halogen
150 oxides. This hypothesis is consistent with observations by Parrish et al. at a mountain station
151 in Colorado, where a missing oxidant of photolytic origin was identified (Parrish et al., 1986).
152 It was shown that if the NO to NO₂ oxidation was completely due to RO_x, the increased O₃
153 production would result in O₃ levels significantly higher than measured, yet if the oxidant
154 exhibited similar reaction mechanisms to IO, extremely high (70 pptV) mixing ratios of IO
155 would be needed (Parrish et al., 1986). These IO levels are more than an order of magnitude
156 higher than observations in the marine atmosphere (Inamdar et al., 2020; Mahajan et al., 2010;
157 Prados-Roman et al., 2015; Read et al., 2008).

158 In regions where the net O₃ production rate (NOPR) is negligible or negative during the
159 day due to very low NO levels, it is more relevant to compare the NOPR to the observed change
160 in [O₃]. The chemical NOPR can be calculated as the difference between the photochemical
161 processes producing and destroying O₃:

$$162 \quad \text{NOPR} = P(\text{O}_3) - L(\text{O}_3) \quad (\text{VII})$$

163 where P(O₃) is determined using equation (VI) and the loss rate of O₃ (L(O₃)), is usually
164 determined from reactions (8-12). Additionally, halogens have previously been shown to cause
165 an O₃ loss of 0.23 ± 0.05 ppbV h⁻¹ in the MBL (initiated by reaction 13) (Read et al., 2008),
166 which is in line with other studies suggesting that halogens can have a significant impact on O₃
167 in marine environments (Saiz-Lopez et al., 2012; Sherwen et al., 2016; Vogt et al., 1999).





174 The actual rate of change of $[O_3]$ within the planetary boundary layer is also impacted
175 by the physical processes of advection, deposition and entrainment, which complicates
176 comparisons with the NOPR. However, if these physical processes change only negligibly over
177 the course of a day, such as in marine well mixed air masses, their net influence can be deduced
178 from the net night time change in O_3 (Ayers and Galbally, 1995; Ayers et al., 1992; Read et
179 al., 2008), allowing a calculation of the NOPR from observations. A comparison of the
180 observed and calculated NOPR gives an indication of whether production and loss rates of O_3
181 from known processes are sufficient to explain the observed O_3 tendency (Read et al., 2008).

182 From the studies shown in Table 1, there is clearly widespread evidence of enhanced
183 PSS-derived RO_2 compared to measurements and models, however, all methods to derive RO_x
184 are not without challenges as described above. The large uncertainties associated with RO_x
185 measurements, especially at high humidities where the chain length is significantly impacted
186 by enhanced wall loss and the production of HNO_3 , suggest that measurements could be
187 underestimating RO_x in the atmosphere. Previous studies also find that the additional
188 conversion of NO to NO_2 caused by the extra “ RO_2 ” should only produce minimal additional
189 O_3 , or at least lead to additional O_3 destruction, thus inferring an unknown missing oxidant
190 which exhibits different chemical behaviour to peroxy radicals.

191 Up to 25% of methane removal occurs in the tropical MBL due to the high
192 photochemical activity and humidity resulting in high OH radical concentrations (Bloss et al.,
193 2005). Thus, it is crucially important to understand the fundamental oxidation processes, such
194 as the NO_x - O_3 cycle, occurring in this region. However, remote NO_x measurements are rare
195 due to the difficulty in measuring very low (pptV) mixing ratios. Most previous remote NO_x
196 measurements have taken place during short campaigns and do not give information on
197 seasonal changes and long-term trends (Carsey et al., 1997; Jacob et al., 1996; Peterson and
198 Honrath, 1999; Rhoads et al., 1997). Here, we investigate the photostationary state under clean

199 marine conditions from three years of observations (2017-2020) at the Cape Verde
200 Atmospheric Observatory (CVAO) in the tropical east Atlantic, representing a unique dataset
201 to investigate NO_x-O₃ chemistry in the remote MBL (Andersen et al., 2021; Carpenter et al.,
202 2010; Lee et al., 2009). We also compare the chemical net O₃ production rate (NOPR)
203 calculated from a box model with NOPR derived from the observed net O₃ rate of change, in
204 order to evaluate the possibility of missing peroxy radicals in this remote environment.

205

206 3 Methods

207 3.1 Measurements

208 Year-round measurements of meteorological parameters and trace gases including NO,
209 NO₂, and C₂-C₈ VOCs have been conducted at the CVAO (16° 51' N, 24° 52' W) since October
210 2006. The CVAO is located on the north eastern coast of São Vicente, Cabo Verde. The air
211 sampled predominantly comes from the northeast (see Figure 1) and has travelled over the
212 Atlantic Ocean for multiple days since the last exposure to anthropogenic emissions, with the
213 potential exception of ship emissions (Carpenter et al., 2010; Read et al., 2008). This makes it
214 an ideal location to investigate fundamental photochemistry in an ultra-clean environment.

215 Wind speed (m/s), wind direction (°), temperature (°C), relative humidity (%),
216 barometric pressure (mbar) and total solar radiation (W/m²) are measured at a height of 7.5 m
217 using an automatic weather station from Campbell Scientific. NO and NO₂ have been measured
218 using an ultra-high sensitivity NO chemiluminescence instrument, which measures NO₂ by
219 photolytic conversion to NO, at the CVAO since 2006 (Lee et al., 2009). The technique and
220 data analysis have been described in detail elsewhere (Andersen et al., 2021). O₃ is measured
221 using a Thermo Scientific 49i Ozone monitor as described in Read et al. (2008). Photolysis
222 rates of a variety of species were measured in 2020 using a spectral radiometer (a 2-pi sr quartz
223 diffuser coupled to an Ocean Optics QE65000 spectrometer via a 10 m fibre optic cable). Prior
224 to 2020, photolysis rates are calculated in this study based on the correlation between the
225 measured photolysis rates in 2020 and the total solar radiation, as described in the
226 supplementary information. Average $j\text{NO}_2$ and $j\text{O}(^1\text{D})$ for different seasons are shown in Table
227 2. VOCs are measured using a dual channel Agilent 7890A gas chromatograph coupled with a
228 Flame Ionization Detector (GC-FID) and a MARKES Thermal Desorption Unit with an ozone
229 precursor trap that is cooled to -30 °C (Read et al., 2009). Details of the calibration and

230 uncertainties are given in the World Calibration Centre (WCC)-VOC audit report
231 (Steinbrecher, 2019). Examples of the VOCs measured at the CVAO can be found in Table 2.
232 Carbon monoxide (CO), and methane (CH₄), are measured using a cavity ring-down
233 spectrometer (CRDS), G2401 manufactured by Picarro Inc, following the Global Atmosphere
234 Watch (GAW) recommended technique for long term remote measurements. The instrument
235 is highly linear, has a precision of 1 ppbV and 0.3 ppbV over 10 minutes for CO and CH₄
236 respectively and no measurable drift (Zellweger et al., 2016; Zellweger et al., 2012).

237 Time series of NO, NO₂, O₃, *j*NO₂, *j*O(¹D), temperature, CO, propene, benzene and
238 CH₄ for July 2017 – June 2020 are shown in figures S4-S6. The specifics of each instrument
239 and their respective measurements can be found in Table 2 and a full description of the CVAO
240 site and associated measurements is given in Carpenter et al. (2010).

241

242 3.1.1 NO₂ Measurement Artefact

243 One of the drawbacks of measuring NO₂ by photolytic conversion to NO is it can be
244 subject to artefacts. These could either be of a photolytic or thermal origin (Bradshaw et al.,
245 1999; Gao et al., 1994; Parrish et al., 1990; Ridley et al., 1988; Ryerson et al., 2000). Photolytic
246 artefacts occur when other compounds containing -NO, -NO₂, or -NO₃ photolyse to form NO
247 over a similar wavelength range as NO₂ and thereby produce an overestimate of NO₂ in the
248 sample (Pollack et al., 2010). Thermal artefacts are caused by thermally labile compounds
249 which decompose in photolytic converters when they heat up and release NO that is measured
250 by the detector or NO₂ which is immediately photolytically converted to NO and then detected
251 (Reed et al., 2016). Additional artefact can arise from compounds sticking to the converter and
252 creating an artefact when the converter is switched on. The potential NO₂ artefact can be
253 estimated using measured or modelled mixing ratios of a range of potential interfering
254 compounds.

255 The photolytic contribution can be estimated based on the absorption cross section
256 (ACS) of NO₂ and the potential interferents around the peak wavelength of the diodes used to
257 convert NO₂ into NO (385 ± 5 nm). The ACS of NO₂ and some known interfering compounds
258 over the wavelength range 380-390 nm are shown in Table 3. NO₂ and most of the interferents,
259 with the exception of HONO, show relatively invariant ACSs across these wavelengths. When
260 the ACSs of both NO₂ and the particular interferent are invariant over the spectral output of the

261 diodes, the ratio at the peak wavelength is used to estimate the potential artefact. However,
262 since the ACS of HONO varies significantly over the range, the HONO/NO₂ ACS ratio has
263 been estimated assuming a Gaussian output of the diodes over the wavelengths. It is also
264 important to take into account whether photolysis of the potential interferent produces NO₂ or
265 NO. If NO is the product, then one converted molecule will be detected as two NO₂ molecules
266 if the conversion efficiency of NO₂ is 50 %. If NO₂ is the product then it will be photolysed to
267 NO with a lower conversion efficiency than NO₂ due to spending less time in the converter
268 than ambient NO₂. However, the conversion efficiency of NO₂ is used here (Table 3) to
269 determine an upper limit of the contribution to the NO₂ artefact. The investigated organic
270 nitrates (C₂H₅ONO₂, CH₃ONO₂, *n*- and *i*-C₃H₇ONO₂, 1- and 2-C₄H₉ONO₂, CH₃O₂NO₂, and
271 CH₃C(O)O₂NO₂), HNO₃, and NO₃ do not photolyse at 385 nm and have therefore not been
272 included in the evaluation of photolytic artefacts (Atkinson et al., 2004).

273 The main potential photolytic artefact for the CVAO NO₂ measurements is HONO.
274 Measurements of HONO at the CVAO using a Long Path Absorption Photometer (LOPAP)
275 show levels of up to ~ 5 pptV (Reed et al., 2017), indicating an NO₂ artefact of up to 0.63 pptV.
276 However, these measurements were made using a thermostated inlet system with reactive
277 HONO stripping, where loss of HONO to the sample lines is minimised. The NO_x instrument
278 at the CVAO samples at the end of the glass manifold making it highly likely that a fraction of
279 HONO is lost on the manifold before the air is introduced to the NO_x instrument due to the
280 high surface reactivity of HONO (Pinto et al., 2014; Syomin and Finlayson-Pitts, 2003). Thus,
281 we regard the potential HONO-induced artefact of 0.63 pptV as an upper limit. No other
282 potential photolytic artefacts have been measured at the CVAO, however using the GEOS-
283 Chem model (see section 3.2.2) we calculated seasonal cycles of 20 potential interfering
284 compounds at the CVAO (Figure S7). None of these compounds exhibit major seasonal
285 differences, indicating that any measurement artefact will be fairly constant across the year.
286 The contribution from photolytic degradation of compounds other than HONO is predicted to
287 be less than 0.05 pptV using the estimated conversion efficiency of each compound in Table 3
288 and the modelled mixing ratios at the CVAO.

289 Peroxyacetyl nitrate (PAN) is produced in polluted areas and transported to remote
290 regions, where it can thermally decompose into peroxy radicals and NO₂. 5.8% of the available
291 PAN has been shown to thermally decompose in blue light converters (BLC) switched on 40%
292 of the time (Reed et al., 2016). This can cause significant overestimations of NO₂ in colder
293 regions where PAN can build up in the atmosphere due to its long lifetime (Kleindienst, 1994),

294 however, in warmer regions such as Cabo Verde the overestimation will be substantially lower
295 due to the much shorter lifetime (~ 40-230 minutes at 25°C) (Bridier et al., 1991; Kleindienst,
296 1994), and hence lower concentration of PAN. At the CVAO, PAN was measured in February
297 2020 using gas chromatography as described by Whalley et al. (Whalley et al., 2004), however,
298 all measurements were below the limit of detection (LOD) of 6 pptV. We measured the
299 temperature increase of the air within an identical photolytic converter (PLC) to the one used
300 at the CVAO to be less than 1°C in the laboratory, suggesting a minimal shift in the PAN
301 equilibrium in ambient air. We calculate an increase in NO₂ of 0.28 pptV arising from 6 pptV
302 of PAN when increasing the temperature from 298 K to 299 K. Combining photolytic and
303 thermal artefact contributions gives a maximum potential NO₂ artefact of 0.95 pptV at the
304 CVAO, which is within the uncertainty previously reported for the NO₂ measurements
305 (Andersen et al., 2021), as shown in Table 2.

306

307 3.2 Modelling

308 3.2.1 Chemical Box Modelling

309 A tailored zero-dimensional chemical box model of the lower atmosphere,
310 incorporating a subset of the Master Chemical Mechanism (MCM v3.3.1) (Jenkin et al., 2015)
311 into the AtChem2 modelling toolkit (Sommariva et al., 2020), was used to estimate
312 concentrations of OH, HO₂ and RO₂ and daily chemical production and loss of O₃ at the CVAO.
313 The MCM describes the detailed atmospheric chemical degradation of 143 VOCs, through
314 17,500 reactions of 6900 species. More details can be found on the MCM website
315 (<http://mcm.york.ac.uk>, last access: 4th March 2022). A fixed deposition rate of $1.2 \times 10^{-5} \text{ s}^{-1}$
316 was applied to all model generated species, giving them a lifetime of approximately 24 hours.
317 The model was constrained to 34 observationally derived photolysis rates, temperature,
318 pressure, and relative humidity, along with a range of observed chemical species, defined in
319 Table 2.

320 While the box model is constrained to a variety of VOCs, which are expected to be the
321 most dominant at the CVAO, it is only constrained to two oxygenated VOCs (OVOCs);
322 methanol and acetone, due to the lack of reliable measurements of other OVOCs. Acetaldehyde
323 and formaldehyde are expected to be the dominant OVOCs not constrained in the box model.
324 Acetaldehyde from the ATom aircraft campaigns in October 2017, May 2018, and August 2018
325 show levels of between ~150 and ~250 pptV (Wofsy et al., 2021), which agrees well with

326 average observations of 180 pptV in the northern hemisphere over the Atlantic Ocean (Yang
327 et al., 2014). Formaldehyde measured at the CVAO in 2006-2007 varied from 350 to 550 pptV
328 (Mahajan et al., 2011). Compared to using the levels generated by the box model of ~8 pptV
329 of acetaldehyde and 270 pptV of formaldehyde, constraining these gases to 150 pptV and 450
330 pptV, respectively, increases the total RO_x levels by 3% from 52.7 pptV to 54.4 pptV. Thus,
331 we consider that the major VOCs and OVOCs are constrained sufficiently well in the box
332 model for the purpose of simulating HO₂ and RO₂ levels.

333

334 3.2.2 GEOS-Chem

335 Concentrations of 20 different chemical species were extracted every hour during 2019
336 at nearest point in space and time from the GEOS-Chem model (v12.9.0,
337 DOI:10.5281/zenodo.3950327). The v12.9.0 model as described by Wang et al. (2021) was run
338 at a nested horizontal resolution of 0.25x0.3125 degrees over the region (-32.0 to 15.0 °E, 0.0
339 to 34.0 °N), with boundary conditions provided by a separate global model run spun up for one
340 year and with acid uptake on dust considered as described by Fairlie et al. (2010) (Fairlie et al.,
341 2010; Wang et al., 2021).

342

343 4 Results and Discussion

344 Monthly diurnal cycles of HO₂, RO₂, and OH were modelled by constraining the box
345 model to the measurements described in Table 2 (except NO₂) using hourly median
346 concentrations for each month from July 2017 – June 2020 where all the trace gas
347 measurements were available. When measured *j*O(¹D) was not available, the hourly average
348 from the same month across the other years was used. Calculated photolysis rates based on
349 total solar radiation (see supplementary) were used up to December 2019 for all other
350 photolysis rates than *j*O(¹D).

351 The modelled OH, HO₂ and RO₂ concentrations agree reasonably well with previous
352 measurements from short term field campaigns based at the CVAO and from various cruises
353 in the Atlantic Ocean (see Figure 2). All the previous measurements of RO_x (HO₂ + RO₂)
354 shown in Figure 2 were conducted using the chemical amplifier technique, which is subject to
355 high uncertainties due to the challenges described above. The box modelled RO₂ shows a strong

356 correlation with the measured $j\text{O}(^1\text{D})$, but no correlation to CO (pollution tracer) or CH_4 , which
357 is expected to be the primary precursor. Daily diurnal cycles of RO_2 and HO_2 for 9 days in
358 August 2017, 12 days in October 2017, and 20 days in January 2018 were modelled to
359 investigate their daily variability (see Figure S8). Seasonal differences can be observed from
360 the daily outputs, but no major day to day changes within a given month.

361

362 4.1 Comparison of measured and PSS NO_2 concentrations

363 Daily midday (12.00-15.00 UTC, local+1) NO_2 mixing ratios were calculated from the
364 Leighton ratio using equation II ($[\text{NO}_2]_{\text{PSS}}$), the measured NO, O_3 , and $j\text{NO}_2$ and $k_1 = 2.07 \times$
365 $10^{-12} \times e^{(-1400/T)}$ (Atkinson et al., 2004) for a three-year period (July 2017 – June 2020).
366 Individual uncertainties of $[\text{NO}_2]_{\text{PSS}}$ were determined to be 4.20 ± 3.74 pptV (1σ) for each day
367 using the 2σ hourly uncertainties for all the used measurements, which is very similar to the
368 uncertainty of hourly measured $[\text{NO}_2]$ (Table 2). Figure 3A shows that $[\text{NO}_2]_{\text{PSS}}$ significantly
369 underestimates the measured NO_2 , indicating that additional oxidants are needed to convert
370 NO into NO_2 . Daily midday values of $[\text{NO}_2]_{\text{PSS ext.}}$ were calculated using equation III, where a
371 midday average of each modelled monthly diurnal cycle of HO_2 and RO_2 in Figure 2 was used
372 for all days of their respective month together with previous yearly averaged midday
373 measurements of IO (1.4 ± 0.8 pptV, 1σ) and BrO (2.5 ± 1.1 pptV, 1σ) (Mahajan et al., 2010;
374 Read et al., 2008) at the CVAO. RO_2 was assumed to be equivalent to CH_3O_2 , making $k_4 = 2.3$
375 $\times 10^{-12} \times e^{(360/T)}$, $k_5 = 3.45 \times 10^{-12} \times e^{(270/T)}$, $k_6 = 7.15 \times 10^{-12} \times e^{(300/T)}$, and $k_7 = 8.7 \times 10^{-12} \times$
376 $e^{(260/T)}$ (Atkinson et al., 2004). Uncertainties for each estimation of $[\text{NO}_2]_{\text{PSS ext.}}$ were
377 determined using the calculated 2σ hourly uncertainties on the measurements and a 20%
378 uncertainty on all rate coefficients. This gives a total average uncertainty of 4.90 ± 4.12 pptV
379 (1σ), excluding any uncertainties in $[\text{HO}_2]$ and $[\text{RO}_2]$. $[\text{NO}_2]_{\text{PSS ext.}}$ was calculated using a
380 midday average of the modelled monthly $[\text{HO}_2]$ and $[\text{RO}_2]$ in Figure 2 as well as the modelled
381 daily midday averages from the diurnal cycles in Figure S8 for August 2017, October 2017,
382 and January 2018. A scatter plot of monthly vs daily calculated $[\text{NO}_2]_{\text{PSS ext.}}$ around the 1:1 line
383 (see Figure S9) verifies the use of monthly calculated $[\text{HO}_2]$ and $[\text{RO}_2]$ for the remaining
384 analyses.

385 Figure 3B shows that the agreement between measured and predicted NO_2 was
386 improved significantly by including modelled additional oxidants with the slope of the linear
387 fit increasing from 0.48 to 0.71. The coefficient of determination was similar for both plots:

388 Figure 3A, $r^2 = 0.81$ and Figure 3B, $r^2 = 0.77$. We next investigate whether the mixing ratio of
389 NO influences the ability of the full PSS equation (equation III) to predict NO₂. Daily midday
390 averages of $[\text{NO}_2]_{\text{Obs.}}/[\text{NO}_2]_{\text{PSS ext.}}$ are plotted as a function of NO in Figure 4. A ratio of 1
391 would be expected if all relevant reaction mechanisms have been taken into account. The
392 deviations from 1 in the ratio can be observed to increase with decreasing NO mixing ratio
393 during March-December. The dashed lines in Figure 4 visualise the effect of a constant NO₂
394 artefact of 0.95 pptV (our calculated upper limit) on the $[\text{NO}_2]_{\text{Obs.}}/[\text{NO}_2]_{\text{PSS ext.}}$ ratio, showing
395 that the artefact, while small, can explain some of this observed trend. However, only a small
396 dependence on the NO mixing ratio is seen for January and February, where enhancements of
397 $[\text{NO}_2]_{\text{Obs.}}/[\text{NO}_2]_{\text{PSS ext.}}$ above 1 continue out to 10 pptV of NO. At Hohenpeissenberg, Germany,
398 similar trends with increasing NO₂/NO ratio with decreasing NO have been observed, which
399 were partly explained by measurement uncertainty in NO and partly by the PSS not being
400 established after being perturbed by NO_x emissions or variable $j\text{NO}_2$ (Mannschreck et al.,
401 2004). An opposite trend to that observed here and at Hohenpeissenberg was observed over the
402 South Atlantic Ocean, with increasing deviations in $[\text{NO}_2]_{\text{Obs.}}/[\text{NO}_2]_{\text{PSS ext.}}$ with increasing NO₂
403 from 3-20 pptV (Hosaynali Beygi et al., 2011), which was explained by a missing photolytic
404 oxidation process.

405

406 4.2 NO₂ Artefact or Missing Oxidant?

407 Deviations between $[\text{NO}_2]_{\text{Obs.}}$ and $[\text{NO}_2]_{\text{PSS ext.}}$ are usually attributed to an unaccounted
408 artefact in the NO₂ measurements or a missing oxidant converting NO into NO₂ (Bradshaw et
409 al., 1999; Carpenter et al., 1998; Crawford et al., 1996; Hauglustaine et al., 1999; Hauglustaine
410 et al., 1996; Hosaynali Beygi et al., 2011; Volz-Thomas et al., 2003). As discussed above, we
411 show that below 5 pptV of ambient NO, our calculated maximum NO₂ artefact of 0.95 pptV
412 starts to have an impact on the $[\text{NO}_2]_{\text{Obs.}}/[\text{NO}_2]_{\text{PSS ext.}}$ ratio, however, it is not enough to explain
413 the enhancements observed, especially in wintertime at the CVAO.

414 The production of RO₂ and HO₂ radicals is dependent on the abundance of their VOC
415 and CO precursors as well as on photochemical activity. To investigate whether the availability
416 of VOCs, CO or sunlight was related to the discrepancy between $[\text{NO}_2]_{\text{Obs.}}$ and $[\text{NO}_2]_{\text{PSS ext.}}$,
417 boxplots of the $[\text{NO}_2]_{\text{Obs.}}/[\text{NO}_2]_{\text{PSS ext.}}$ ratio are plotted as a function of intervals of the mixing
418 ratio of different precursors and $j\text{NO}_2$ (Figure 5). The high deviations in $[\text{NO}_2]_{\text{Obs.}}/[\text{NO}_2]_{\text{PSS ext.}}$
419 can be observed to be associated with higher measured mixing ratios of CO, ethane, and

420 acetylene. No obvious trend can be observed in the dependence on $j\text{NO}_2$, contrast to Hosaynali
421 Beygi et al. (2011), who observed increasing deviations in $[\text{NO}_2]_{\text{Obs.}}/[\text{NO}_2]_{\text{PSS ext.}}$ with
422 increasing $j\text{NO}_2$. However, it should be noted that midday $j\text{NO}_2$ at the sub-tropical CVAO
423 shows relatively little seasonal variation. Figure 5 shows that the abundances of ethene and
424 propene, both of which have atmospheric lifetimes of less than 3 days, do not seem to affect
425 the deviation of $[\text{NO}_2]_{\text{Obs.}}/[\text{NO}_2]_{\text{PSS ext.}}$ from 1. Conversely, high abundances of CO, ethane, and
426 acetylene, which all have atmospheric lifetimes above 6 weeks (Atkinson et al., 2006), are
427 observed to be associated with higher $[\text{NO}_2]_{\text{Obs.}}/[\text{NO}_2]_{\text{PSS ext.}}$ ratios. This could indicate that
428 long-range transport of pollutants supplies additional peroxy radicals (or other NO to NO_2
429 oxidants) at the CVAO, which are not predicted from known sources and photochemistry.

430 To further evaluate the impact of pollution, $[\text{NO}_2]_{\text{Obs.}}/[\text{NO}_2]_{\text{PSS ext.}}$ was separated into
431 three categories based on CO mixing ratios; $\text{CO} < 90$ ppbV, $90 \text{ ppbV} < \text{CO} < 100$ ppbV, and
432 $\text{CO} > 100$ ppbV. The deviations of $[\text{NO}_2]_{\text{Obs.}}/[\text{NO}_2]_{\text{PSS ext.}}$ from 1 increase with increasing [CO],
433 with 50th (25th-75th) percentiles of 1.10 (0.82 -1.37) for $\text{CO} < 90$ ppbV, 1.20 (0.97-1.54) for 90
434 $\text{ppbV} < \text{CO} < 100$ ppbV, and 1.50 (1.18-1.78) for $\text{CO} > 100$ ppbV. The small deviation from
435 1, which is within the uncertainty of our measurements (see below), for $\text{CO} < 90$ ppbV is strong
436 evidence that fundamental oxidation process in ultra-clean marine air, where the main
437 precursors of RO_2 and HO_2 are CH_4 and CO giving CH_3O_2 and HO_2 , respectively, are well
438 understood.

439 An NO_2 artefact of 0.7 pptV would reduce the ratio of 1.10 to 1.00 in air masses with
440 $\text{CO} < 90$ ppbV. Since the minimum value of the artefact is 0 pptV (if there was no conversion
441 of interferent compounds to NO or NO_2), and our estimated upper limit is 0.97 pptV, we
442 therefore consider it a reasonable assumption that the average NO_2 artefact of our instrument
443 at the CVAO is 0.7 pptV. We make the simple *a priori* assumption that this applies across all
444 measurements during the period of analyses. Such an artefact is insignificant when considering
445 total NO_x concentrations, however, it has a non-negligible impact when investigating NO_2/NO
446 ratios in this very low NO_x environment.

447 Subtracting 0.7 pptV from all the NO_2 observations results in median (25th-75th
448 percentiles) ratios of 1.00 (0.76-1.29) for $\text{CO} < 90$ ppbV, 1.14 (0.89-1.47) for $90 \text{ ppbV} < \text{CO}$
449 < 100 ppbV, and 1.42 (1.12-1.68) for $\text{CO} > 100$ ppbV (Table 4). A student's t-test was
450 performed to evaluate whether the two categories where $\text{CO} < 90$ ppbV and $\text{CO} > 100$ ppbV
451 were significantly different. A mean and standard deviation of 1.06 and 0.42 for $\text{CO} < 90$ ppbV

452 and 1.45 and 0.61 for $\text{CO} < 100$ ppbV results in a t-value of 6.59, which makes the two
453 categories statistically different. Distributions of each category are plotted in Figure 6A. When
454 CO is between 90 and 100 ppbV, the distribution of $[\text{NO}_2]_{\text{Obs.}}/[\text{NO}_2]_{\text{PSS ext.}}$ shows the highest
455 occurrences at ratios of ~ 1 and ~ 1.5 . When $\text{CO} > 100$ ppbV, it is evident that either additional
456 oxidants are needed to convert NO to NO_2 , or an additional NO_2 artefact of the order of 4.4
457 pptV is present in these air masses. As an artefact of 0.7 pptV has already been subtracted, and
458 measurements of HONO and PAN and modelled mixing ratios of halogen nitrates indicate a
459 fairly stable artefact across the year, 4.4 pptV of additional artefact seems highly unlikely. This
460 leaves the possibility of a missing oxidant when the sampled air is enhanced in CO .

461 Using equation (IV) and (V), the required RO_x ($\text{RO}_2 + \text{HO}_2$) and XO ($\text{IO} + \text{BrO}$)
462 concentrations needed to reconcile $[\text{NO}_2]_{\text{Obs.}}$ with $[\text{NO}_2]_{\text{PSS ext.}}$ can be estimated using $k_{4,5} = 2.3$
463 $\times 10^{-12} \times e^{(360/T)}$ and $k_{6,7} = 8.7 \times 10^{-12} \times e^{(260/T)}$ (Atkinson et al., 2004). Our calculations are based
464 on two scenarios: (1) that the measured $[\text{BrO}]$ and $[\text{IO}]$ are correct and there is unaccounted for
465 RO_x , or (2) that the modelled $[\text{RO}_x]$ is correct and there is more $[\text{XO}]$ than measured. Due to
466 the similar rate coefficients for IO and BrO reacting with NO , a combined XO can be estimated.
467 The results are summarised in Table 4 based on the three CO categories. The median required
468 RO_x was determined to be 65.0 (33.68 - 112.5, 25th-75th percentile) pptV and 109.7 (63.14 -
469 149.5, 25th-75th percentile) pptV for $90 \text{ ppbV} < \text{CO} < 100 \text{ ppbV}$ and $\text{CO} > 100 \text{ ppbV}$,
470 respectively. RO_x measurements during the ALBATROSS cruise varied from 40-80 pptV
471 while in the North Atlantic, however, with a reported uncertainty of 25% (1σ) they could be as
472 high as 100 pptV (Burkert et al., 2001). Such concentrations are comparable to the required
473 median RO_x in this study of 109.7 pptV when $\text{CO} > 100$ ppbV. The uncertainty reported for
474 ALBATROSS is similar to many other studies which have reported 10-36% uncertainty on
475 chemical amplification RO_x measurements (Cantrell et al., 1997; Clemitshaw et al., 1997;
476 Handisides et al., 2003; Hernández et al., 2001; Hosaynali Beygi et al., 2011; Volz-Thomas et
477 al., 2003), however, a recent study in the Pearl River Delta reported an uncertainty of 60% (1σ)
478 (Ma et al., 2017). This combined with measurements up to ~ 150 pptV of RO_x in the South
479 Atlantic Ocean (Hosaynali Beygi et al., 2011) indicates that our required RO_x levels of ~ 100
480 pptV may not be unrealistic in the MBL.

481 The median required RO_x ($[\text{RO}_x]_{\text{PSS}}$) can be observed to be ~ 2.5 times higher than the
482 levels estimated using the box model for air masses where $\text{CO} > 100$ ppbV, whereas the
483 required $[\text{XO}]$ is a factor of ~ 6.5 higher than previous observations at the CVAO (Mahajan et
484 al., 2010; Read et al., 2008). Across the three categories, the daily median ratio of

485 $[\text{RO}_x]_{\text{PSS}}/[\text{RO}_x]_{\text{Model}}$ is 1.5, which is similar to those observed in previous studies both in remote
 486 and rural regions (see Table 1). The additional XO required to reconcile $[\text{NO}_2]_{\text{Obs.}}$ with
 487 $[\text{NO}_2]_{\text{PSS ext.}}$ was determined for each CO category by subtracting the previous measured
 488 average concentration of 3.9 pptV (2.5 pptV BrO + 1.4 pptV IO) (Read et al., 2008) from the
 489 required XO. Since CO, the main precursor for HO_2 , is constrained by measurements in the
 490 model, the calculated $[\text{HO}_2]$ is assumed to be correct. Thus, we estimate the required and
 491 unaccounted for RO_2 assuming it is all in the form of CH_3O_2 from:

$$492 \quad [\text{RO}_2]_{\text{Required}} = \frac{j\text{NO}_2[\text{NO}_2] - (k_1[\text{O}_3] + k_5[\text{HO}_2] + k_6[\text{IO}] + k_7[\text{BrO}])[\text{NO}]}{k_4[\text{NO}]} \quad (\text{VIII})$$

$$493 \quad [\text{RO}_2]_{\text{Unaccounted}} = \frac{j\text{NO}_2[\text{NO}_2] - (k_1[\text{O}_3] + k_5[\text{HO}_2] + k_6[\text{IO}] + k_7[\text{BrO}])[\text{NO}]}{k_4[\text{NO}]} - [\text{RO}_2]_{\text{model}} \quad (\text{IX})$$

494 Figures 6B and C, show that the unaccounted for RO_2 or XO level increases with
 495 increasing $[\text{CO}]$, reaching a median of 61.3 pptV and 22.7 pptV, respectively, for air masses
 496 where $\text{CO} > 100$ ppbV, which is approximately 2.2 times the box modelled RO_2 and 5.5 times
 497 the measured XO in the same air masses. Such an increase in organic peroxy radicals would,
 498 under more polluted conditions, cause a major increase in O_3 production during a day (Volz-
 499 Thomas et al., 2003). We next examine the impact of additional RO_2 on the net O_3 production
 500 rate in Cabo Verde.

501

502 4.3 Chemical O_3 Loss

503 The daily chemical loss of O_3 between 09.30 (09.00-10.00) and 17.30 (17.00-18.00)
 504 UTC was used to evaluate whether the PSS-derived $[\text{RO}_2]$ was consistent with the net chemical
 505 destruction of O_3 at the CVAO. As discussed above, the measured O_3 mixing ratio in the MBL
 506 is affected by loss mechanisms in the form of photolysis, reactions with HO_x and halogens, and
 507 deposition, and by production through NO_2 photolysis and by entrainment from the O_3 -
 508 enriched free troposphere. Due to the very stable meteorological condition of the MBL, the
 509 variability in entrainment and deposition between night and day is expected to be negligible
 510 (Ayers and Galbally, 1995; Ayers et al., 1992; Read et al., 2008). A combined
 511 entrainment/deposition term can therefore be estimated from night time O_3 measurements,
 512 when there is no photochemical production or loss. An hourly entrainment/deposition term was
 513 determined for each month using the average change in O_3 between 22.30 (22.00-23.00) and
 514 03.30 (03.00-04.00), and found to vary from 0.18 ppbV h^{-1} in January to 0.35 ppbV h^{-1} in May,

515 which is in good agreement with previous measurements at the CVAO of 0.18-0.48 ppbV h⁻¹
516 (Read et al., 2008). The observed daily change in O₃ ($\Delta O_{3 \text{ obs.}}$) (09.30-17.30) was determined
517 to be -0.40 ± 0.32 ppbV h⁻¹ (1 σ) across the three years (2017-2020), which is almost identical
518 to the -0.41 ± 0.33 ppbV h⁻¹ (1 σ) observed at the CVAO in 2007 (Read et al., 2008), but roughly
519 2 times the daily $\Delta O_{3 \text{ obs.}}$ in baseline air at Cape Grim (-0.24 ± 0.32 ppbV h⁻¹, 1 σ) and Mace
520 Head (-0.20 ± 0.21 ppbV h⁻¹, 1 σ) (Carpenter et al., 1997) and 2-40 times the modelled O₃ loss
521 at Mauna Loa (-0.01 to -0.21 ppbV h⁻¹) (Cantrell et al., 1996; Ridley et al., 1992).

522 By subtracting the monthly average entrainment/deposition term from the observed
523 daily ΔO_3 , the daily chemical loss of O₃, $\Delta O_{3 \text{ chem.}}$, is obtained. The observations were filtered
524 to exclude periods where the change in CO concentration over the interval period, ΔCO , was
525 outside 1 standard deviation of the mean ΔCO , to avoid the ΔO_3 determination being affected
526 by changing air masses. The resulting observed chemical loss of O₃ is averaged by month and
527 plotted in black in Figure 7. $\Delta O_{3 \text{ chem.}}$ can be observed to follow photochemical activity, with
528 the lowest $\Delta O_{3 \text{ chem.}}$ in October-February, where the lowest photolysis rates are measured (see
529 supplementary and Table 2) and highest $\Delta O_{3 \text{ chem.}}$ in March-May and September. A small
530 decrease in $\Delta O_{3 \text{ chem.}}$ in June-August occurred simultaneously to the small drop in photolysis
531 rates in June-August. Overall, $\Delta O_{3 \text{ chem.}}$ varied from -0.48 ppbV h⁻¹ in January to -0.88 ppbV h⁻¹
532 in May.

533 In order to evaluate whether these observationally-derived chemical loss rates of O₃ are
534 consistent with PSS-derived peroxy radical concentrations, $\Delta O_{3 \text{ chem.}}$ was estimated using a
535 chemical box model incorporating the MCM, as described in section 3.2.1. The model was
536 constrained to all the measurements described in Table 2, except NO₂ and O₃, which were left
537 unconstrained. $\Delta O_{3 \text{ chem.}}$ was simulated with box modelled [RO₂] and [HO₂], with (blue line in
538 Figure 7) and without (grey in Figure 7) inclusion of the halogen chemistry described in Table
539 S1, allowing an evaluation of the O₃ loss due to halogens, as previously discussed by Read et
540 al. (2008). Simulations were also performed with [CH₃O₂] constrained to the required RO₂,
541 box modelled [HO₂] and including halogen chemistry (orange in Figure 7). In model runs with
542 halogen chemistry, BrO and IO were constrained to previously measured annual averages \pm
543 reported uncertainties (blue shaded area in Figure 7) (Read et al., 2008). Diurnal cycles of the
544 required RO₂ were constructed using the median of the daily midday averages for each month
545 determined using equation (VIII) for the peak concentration at midday, 1 pptV overnight and
546 interpolating linearly in between.

547 Figure 7 shows that all three modelled ΔO_3 chem. exhibited very similar seasonality as
548 the observed ΔO_3 chem.. The difference between running the box model with and without
549 halogen chemistry was 0.24 ± 0.02 ppbV h⁻¹ (1 σ), which is almost equivalent to the results of
550 Read et al. (2008) from the CVAO of 0.23 ± 0.05 ppbV h⁻¹ (1 σ). From May-December, the box
551 modelled ΔO_3 chem. was almost identical whether using modelled RO₂ or constraining CH₃O₂
552 to the required RO₂, and both were very similar to observed ΔO_3 chem.. The largest difference in
553 ΔO_3 chem. between using box modelled RO₂ and constraining CH₃O₂ is observed in January
554 where the difference reached 0.09 ppbV h⁻¹, however, this is caused by constraining CH₃O₂ to
555 100 pptV, which is 5 times more than the modelled RO₂. The average difference between the
556 observed and box modelled ΔO_3 chem. is 0.06 ± 0.07 ppbV h⁻¹ (1 σ) when constraining CH₃O₂ to
557 the required RO₂ and 0.04 ± 0.07 ppbV h⁻¹ (1 σ) when using box modelled RO₂.

558 Overall, the very small differences in modelled ΔO_3 chem. whether including the
559 unaccounted for RO₂ or not are a function of the highly NO_x-limited conditions of the remote
560 MBL, where O₃ production is relatively insensitive to the mixture and abundance of peroxy
561 radicals (Sillman, 1999). Thus, although our analysis shows that peroxy radicals with the
562 equivalent O₃ production potential as CH₃O₂ cannot be ruled out as the missing oxidant in
563 marine air masses with aged pollution, neither does it provide robust evidence that the missing
564 oxidant is O₃-producing. Nevertheless, the deviation between PSS-derived peroxy radicals in
565 this study and previous measurements can potentially be explained by the difficulty in
566 measuring peroxy radicals, as discussed above. This would have important consequences for
567 our understanding of O₃ production under higher NO_x conditions.

568

569 5 Conclusions

570 In the remote MBL (CO < 90 ppbV, NO_x < 43 pptV (90th percentile = 23 pptV)) we
571 have shown that the observed NO₂/NO ratio is consistent with fundamental photochemical
572 theory, and that neither missing oxidants nor deviations of the photostationary state are required
573 to reconcile observations with the calculated NO₂/NO ratio. This is to our knowledge the first
574 time this has been shown in a low NO_x environment. However, observed NO₂ levels became
575 increasingly higher than predicted as the CO mixing ratio increased and the air more influenced
576 by long range transport of air pollution in winter. A detailed analysis of potential NO₂
577 measurement artefacts at the CVAO showed that such artefacts were unlikely to account for
578 these deviations, thus we evaluated the case for a missing NO to NO₂ oxidant. The required

579 oxidant in air masses with CO > 100 ppbV reached a median of 109.7 pptV when treated as
580 CH₃O₂. These levels are ~ 2.5 times higher than both our box modelled RO_x (RO₂ + HO₂) and
581 previous measurements of RO_x measured by chemical amplification at the CVAO. However,
582 chemical amplification measurements are known to be highly uncertain due to the difficulty in
583 determining the chain length of the mixture of RO₂ in the ambient matrix, and we note that the
584 box modelled O₃ production at the CVAO, with the inclusion of these additional peroxy
585 radicals, did not deviate significantly from the observed O₃ production. Overall, we conclude
586 that there is strong evidence for a missing oxidant in remote marine air impacted by long range
587 transport of pollution, and that peroxy radicals cannot be ruled out as to their identity.

588

589 6 Acknowledgements

590 The authors would like to thank the UK Natural Environment Research Council/
591 National Centre for Atmospheric Science (NERC/NCAS) through the Atmospheric
592 Measurement and Observation Facility (AMOF) for funding the CVAO programme. STA's
593 PhD was supported by the SPHERES Natural Environment Research Council (NERC)
594 Doctoral Training Partnership (DTP), under grant NE/L002574/1. LJC acknowledges funding
595 from the European Research Council (ERC) under the European Union's Horizon 2020 pro-
596 gramme (project O3-SML; grant agreement no. 833290).

597

598 7 Author Contributions

599 Data analysis has been performed by STA. The box model has been run by BSN. Back
600 trajectories have been modelled by MR. GEOS-Chem has been run by TS. The instruments at
601 the CVAO have been run by STA, KAR, SP, JH, and LN. KAR and LKW have processed the
602 spectral radiometer data. The manuscript has been written by STA, LJC, JDL, BSN, and KAR.

603

604 8 Additional Information

605 The authors declare that they have no competing interests.

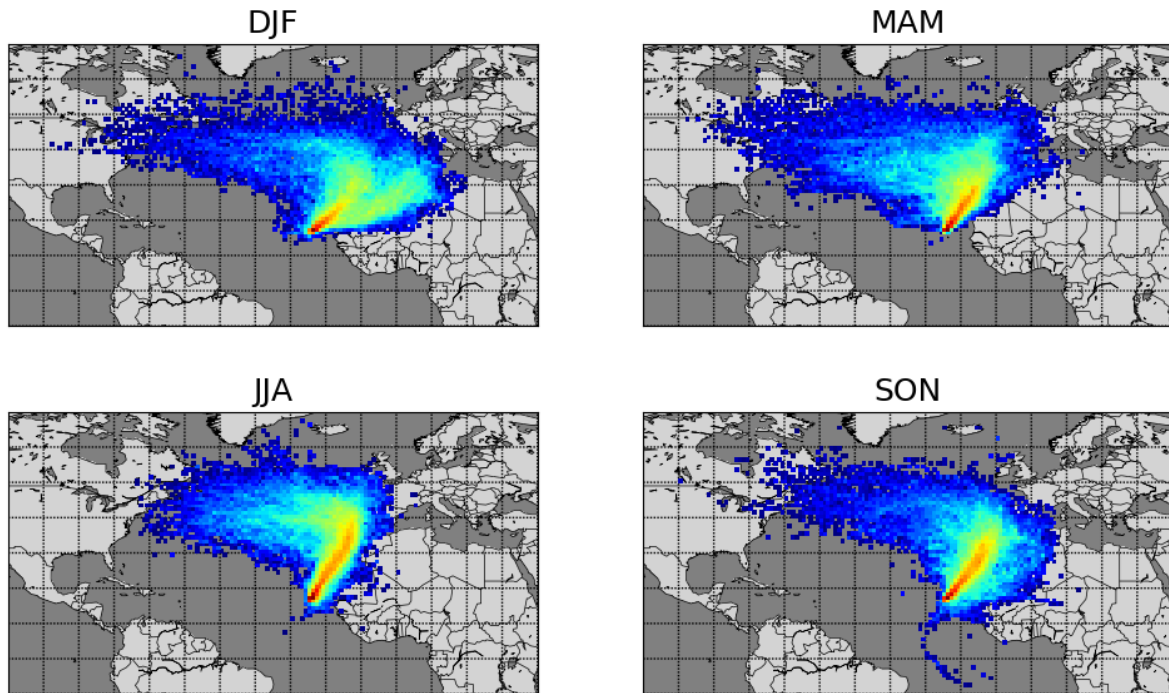
606

607 **8.1 Data availability:**

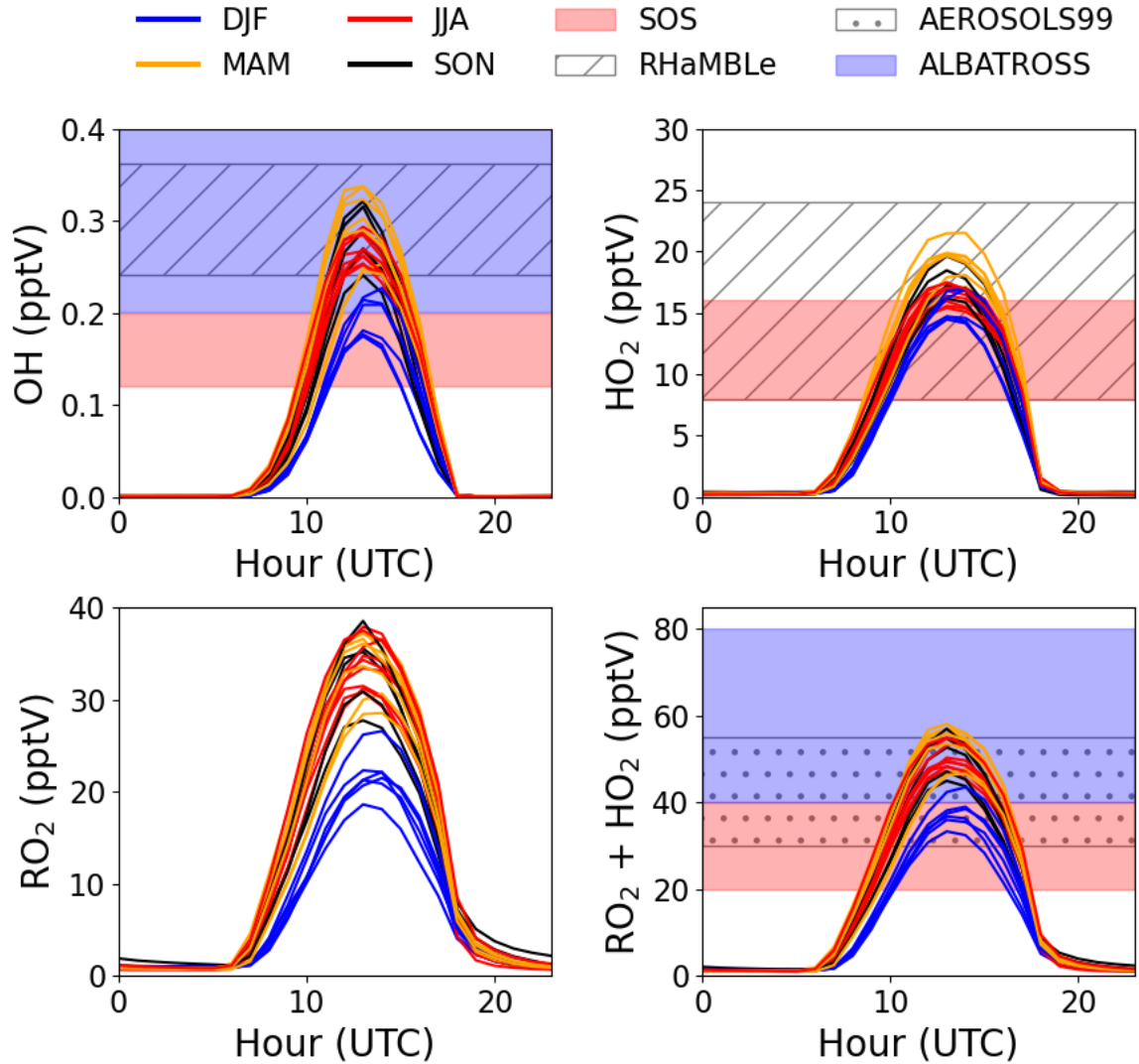
608 NO_x, VOCs, meteorological data, CO and O₃: WDCRG (World Data Centre for
609 Reactive Gases)/Norwegian Institute for Air Research (NILU) EBAS database ([EBAS](http://ebas.nilu.no)
610 [nilu.no](http://ebas.nilu.no))

611 CH₄ and CO: [WDCGG \(World Data Centre for Greenhouse Gases\) \(kishou.go.jp\)](http://kishou.go.jp)

612 9 Figures



613
614 Figure 1: Seasonal average 10-day back trajectories for the CVAO. Locations of released
615 particles are plotted on a $1^\circ \times 1^\circ$ grid, determined using FLEXPART as described in Andersen
616 et al. (2021).



617

618 Figure 2: Average monthly diurnal cycles of modelled OH, HO₂, RO₂, and HO₂+RO₂ coloured
 619 by season compared to midday measurements during SOS (February, May, September, and
 620 November) (Carpenter et al., 2010; Vaughan et al., 2012), RHaMBLe (May and June) (Whalley
 621 et al., 2010), AEROSOLS99 (January and February) (Hernández et al., 2001), and
 622 ALBATROSS (November and December) (Burkert et al., 2001).

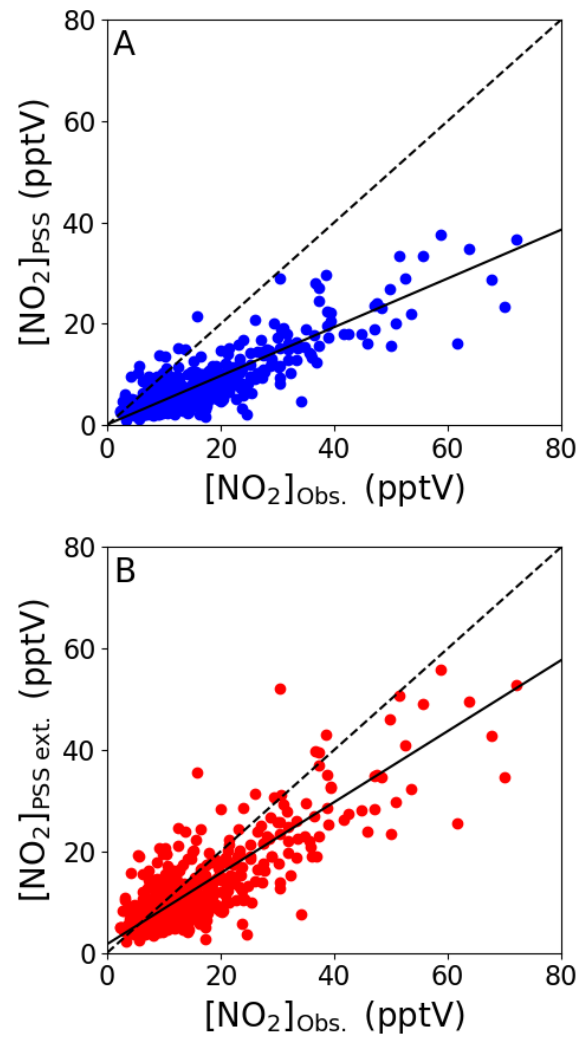
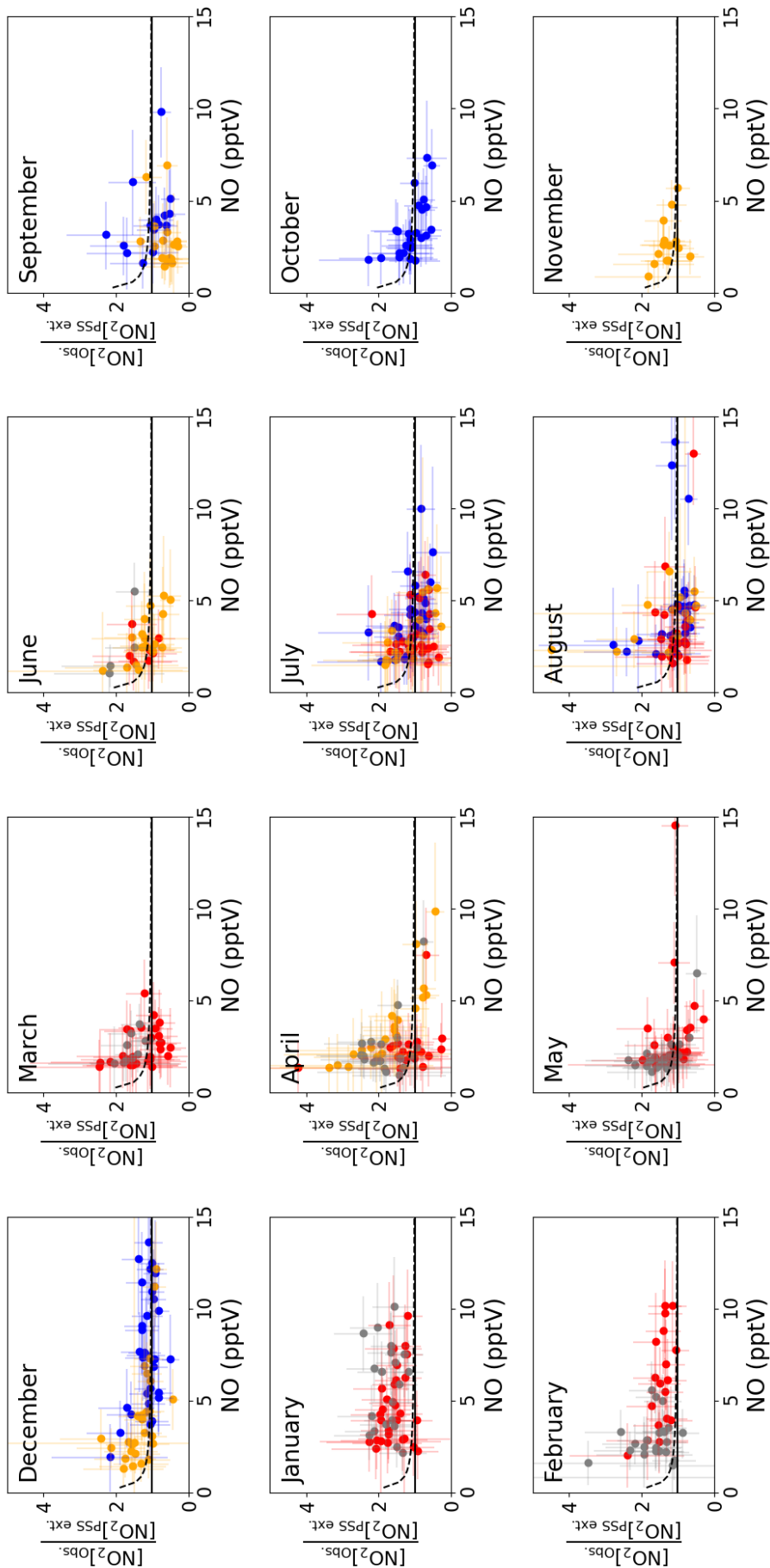
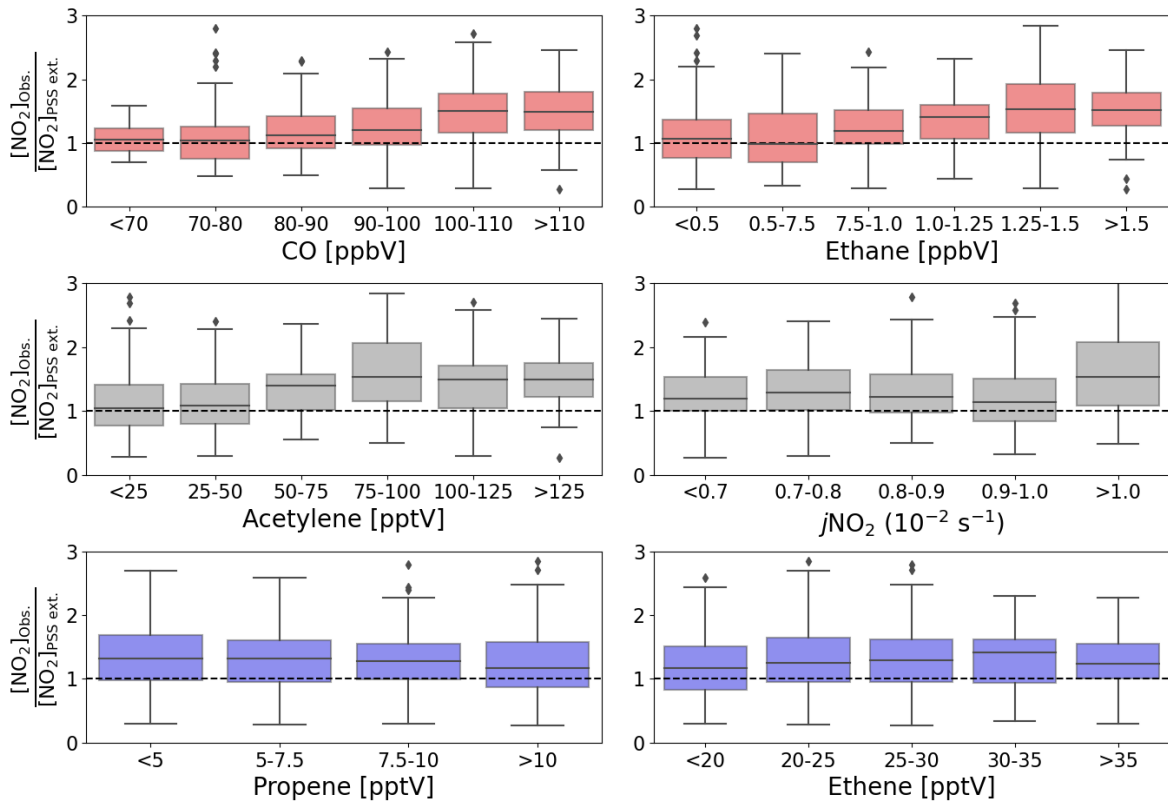


Figure 3: Midday (12.00-15.00 UTC, local+1) daily averages of $[\text{NO}_2]_{\text{PSS}}$ (A) and $[\text{NO}_2]_{\text{PSS ext.}}$ (B) plotted against the observed NO_2 using measurements from July 2017 – June 2020. The black dashed lines show the 1:1 ratio and the solid black lines show the linear fit to the datapoints (A: $0.48 \times [\text{NO}_2]_{\text{Obs.}} + 0.16$, B: $0.70 \times [\text{NO}_2]_{\text{Obs.}} + 1.71$).



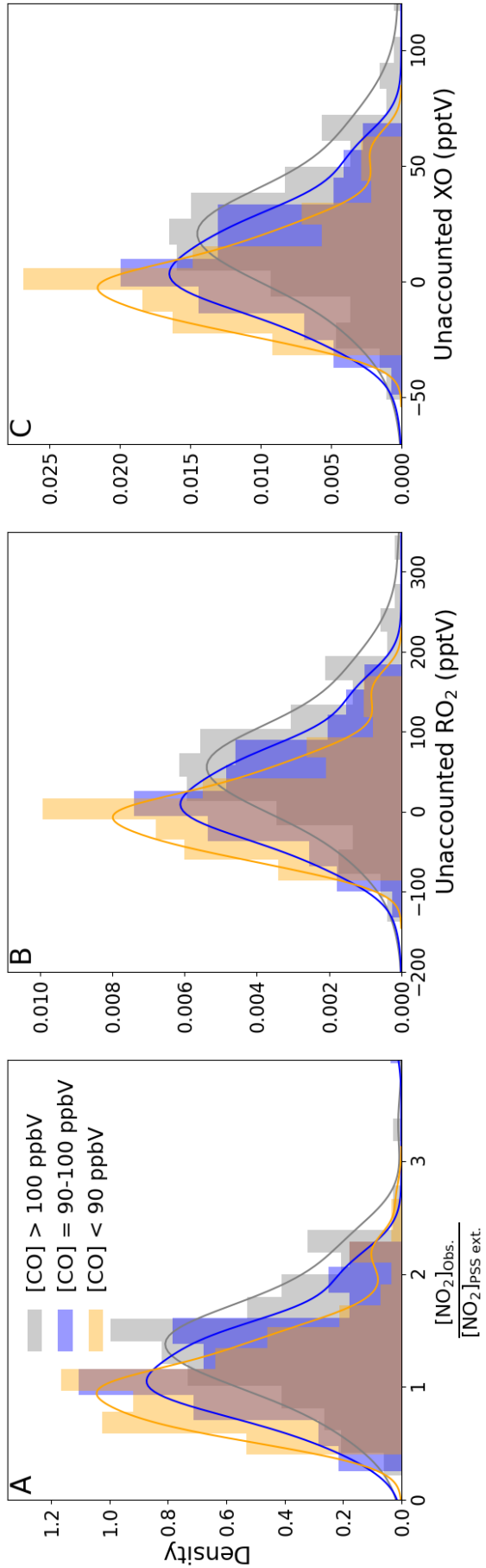
629 Figure 4: Monthly plots of midday (12.00-15.00 UTC, local+1) daily averages of
630 $[\text{NO}_2]_{\text{Obs.}}/[\text{NO}_2]_{\text{PSS ext.}}$ vs. the measured NO mixing ratio. The solid lines represent a ratio of 1
631 between the observed and predicted NO_2 . The error bars represent $\pm 2\sigma$ uncertainty on the
632 calculated ratio and measured NO. The colours represent the year of the measurements: 2017
633 = blue, 2018 = red, 2019 = orange, 2020 = grey. The dashed lines represent $([\text{NO}_2]_{\text{PSS ext.}} + 0.95$
634 $\text{pptV})/[\text{NO}_2]_{\text{PSS ext.}}$ to visualise the effect of a NO_2 artefact of 0.97 pptV on the ratio using the
635 average measured $j\text{NO}_2$ and O_3 and modelled HO_2 and RO_2 for each month and the annually
636 average measured IO and BrO for the CVAO. The uncertainty of each data point has been
637 determined from measurement uncertainties in Table 2, the uncertainties in the measured BrO
638 and IO described in the text, and 20% uncertainty on all the rate coefficients. The uncertainty
639 in the modelled radicals has not been included



640

641 Figure 5: Boxplots of midday (12.00-15.00 UTC, local +1) daily averages of
 642 $[\text{NO}_2]_{\text{obs.}}/[\text{NO}_2]_{\text{PSS ext.}}$ from July 2017 to June 2020 plotted against intervals of five different
 643 measured precursors for either HO_2 or RO_2 and $j\text{NO}_2$. The black dashed lines represent a ratio
 644 of 1.

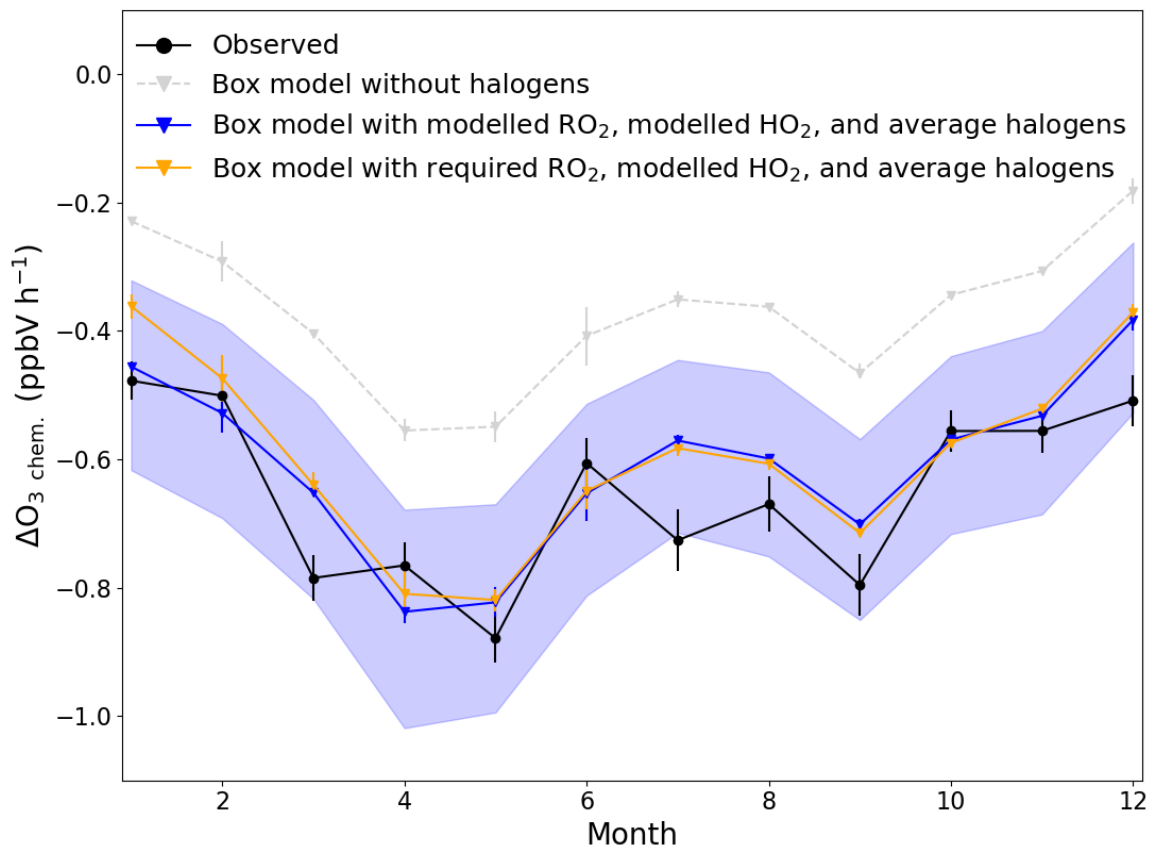
645



647 Figure 6: Density distributions of (A) $[\text{NO}_2]_{\text{Obs.}}/[\text{NO}_2]_{\text{PSS ext.}}$, (B) missing RO_2 , and (C) missing
648 XO separated by measured CO mixing ratios. An NO_2 artefact of 0.7 pptV has been subtracted
649 from all data.

650

651



652

653 Figure 7: Average monthly ΔO_3 due to chemical loss between 09.30 (09.00-10.00) and 17.30
 654 (17.00-18.00) UTC for each month (black) compared to box modelled ΔO_3 due to chemical
 655 loss using modelled RO_2 and HO_2 with (blue) and without (grey) halogen monoxides (BrO and
 656 IO), and using required RO_2 to get $[NO_2]_{Obs.}/[NO_2]_{PSS\ ext.} = 1$, modelled HO_2 , and the annually
 657 averaged halogen monoxides (orange). The error bars on the observed chemical loss is the
 658 standard error of all the days used for each month and for the box model it is the minimum and
 659 maximum ΔO_3 modelled for each month. The blue shaded area show the possible variability
 660 in the chemical loss when including the measured halogens at the CVAO (BrO; 2.5 ± 1.1 pptV,
 661 IO; 1.4 ± 0.8 pptV) (Read et al., 2008).

662

Table 1: Summary of previous studies which have compared $[RO_x]_{PSS}$ against measured and/or modelled $[RO_x]$ in rural, marine and remote conditions.

Location	NO_x instrument	NO_x	ϕ^a	$\frac{[RO_x]_{PSS}}{[RO_x]_{Measured}}$	$\frac{[RO_x]_{PSS}}{[RO_x]_{Model}}$	$\frac{[RO_x]_{Measured}}{[RO_x]_{Model}}$	Reference
Rural conditions							
Hohenpeissenberg, Germany	CLD with PLC ^c	NO_2 : 50-7000 pptV	2-5.7 ^d	2-3 ^e	-	-	(Mannschreck et al., 2004)
Pearl River Delta, China	CLD with PLC ^c	NO_2 : 50-4000 pptV	1-8.5 ^d	~ 1 ^e	2-10	~ 2 ^e	(Ma et al., 2017)
Pabstthum, Germany	CLD with PLC ^c	1-7 ppbV	1.1-3.0 ^d	~ 4 ^e	-	-	(Volz-Thomas et al., 2003)
Idaho Hill, Colorado	CLD with PLC ^c	38 pptV-21.3 ppbV	-	2.1 (mean) ^e	-	~ 1 ^{e, f}	(Cantrell et al., 1997; Williams et al., 1997)
Pine forest, Alabama	CLD with PLC ^c	1-5 ppbV	-	1-2 ^e	-	~ 1 ^{e, f}	(Cantrell et al., 1992; Cantrell et al., 1993a; Parrish et al., 1986)
Essex, England	CLD with Mo ^g	NO_2 : 0.3-9.9 ppbV	-	-	-	~ 1.4 ^e	(Emmerson et al., 2007)
Ponderosa pine forest, Rocky Mountains	CLD with PLC ^c	NO_2 : 100-150 pptV	-	-	-	<3 ^h	(Wolfe et al., 2014)
Marine/Remote with pollution							
Arabian Peninsula	CLD with PLC ^c and CRDS ⁱ	< 50 pptV - > 10 ppbV	-	-	0.95 (median)	-	(Tadic et al., 2020)
Amazon Basin (Manaus)	CLD with PLC ^c	100 pptV - 30 ppbV	1-6 ^d	-	~ 1 ^k	-	(Trebs et al., 2012)
Marine/Remote conditions							
South Atlantic Ocean	CLD with PLC ^c	NO_2 : 3-20 pptV	1-12.5 ^l	1.27 ^e	~ 5	~ 4 ^e	(Hosaynali Beygi et al., 2011)
Mauna Loa, Hawaii	CLD with PLC ^c	20-60 pptV	1.4-2.2	1.5-3 ^e	2-3.5	1.2-2 ^e	(Hauglustaine et al., 1996)
Mace Head, Ireland	CLD with TC ^m	$NO < 10$ pptV	-	-	-	~ 0.25 ^e	(Carpenter et al., 1997; Cox, 1999)
Cape Grim, Tasmania	CLD with PLC ^c	$NO < 5$ pptV	-	-	-	~ 0.4 ^e	(Carpenter et al., 1997; Cox, 1999)
Cabo Verde	CLD with PLC ^c	< 50 pptV	0.45-12.0 ^d (median = 2.1)	-	1.5 (median)	-	This study

665 ^aWithout radicals and halogens. ^b $[RO_x] = [HO_2] + [RO_2]$. ^cCLD with PLC = Detection by
666 chemiluminescence with photolytic converter for NO₂. ^dIncreasing ϕ with decreasing [NO],
667 [NO₂] or [NO_x]. ^e[RO_x] measured by chemical amplification. ^fCalculated/modelled using
668 stead state theory. ^gCLD with Mo = Detection by chemiluminescence with molybdenum
669 converter. ^h[RO_x] measured by Peroxy Radical Chemical Ionization Mass Spectrometry
670 (PeRCIMS). ⁱCRDS = Cavity Ring down spectroscopy. ^kPSS derived [RO_x] was within the
671 range of the modelled values. ^lIncreasing ϕ with increasing [NO₂]. ^mCLD with TC =
672 Detection by chemiluminescence with thermal converter.

Table 2: Overview of instruments and measurements used from the CVAO.

Instrument	Measurement	2 σ Hourly Uncertainty	DJF ^a	MAM ^a	JJA ^a	SON ^a	Reference ^b
AQD	NO (pptV)	1.4 pptV ^c (55 %) ^d	5.3 \pm 7.8	1.9 \pm 4.2	2.7 \pm 5.6	3.6 \pm 5.9	Andersen et al. (2021)
	NO ₂ (pptV)	4.4 pptV ^c (36 %) ^d	27.0 \pm 35.8	10.0 \pm 13.5	10.2 \pm 16.8	10.6 \pm 15.7	
Thermo Scientific 49i	O ₃ (ppbV)	0.07 ppbV ^e (< 1 %)	38.9 \pm 8.8	39.2 \pm 12.1	29.9 \pm 11.9	31.2 \pm 11.1	Read et al. (2008)
Ocean Optics QE650000	<i>j</i> NO ₂ (10 ⁻³ s ⁻¹)	15 %	7.8 \pm 2.7	9.3 \pm 2.2	8.9 \pm 2.5	8.7 \pm 2.4	See supplementary
	<i>j</i> O(¹ D) (10 ⁻⁵ s ⁻¹)	15 %	1.7 \pm 1.2	3.0 \pm 1.3	2.6 \pm 1.2	2.6 \pm 1.2	
Picarro	CO (ppbV)	1.0 ppbV (< 2 %)	99.0 \pm 20.2	103 \pm 17	80.0 \pm 19.3	84.5 \pm 16.6	Zellweger et al. (2012, 2016)
	CH ₄ (ppbV)	0.3 ppbV (< 0.1 %)	1916 \pm 26	1914 \pm 29	1886 \pm 34	1896 \pm 30	
GC-FID	Ethane (pptV)	5.2 %	1438 \pm 600	1204 \pm 608	518 \pm 267	660 \pm 449	
	Ethene (pptV)	5.0 %	31.2 \pm 18.6	23.2 \pm 9.8	27.5 \pm 15.1	28.9 \pm 19.6	
	Acetylene (pptV)	10.7 %	134 \pm 86	86.9 \pm 82.4	22.6 \pm 22.2	38.1 \pm 38.5	
	Propane (pptV)	5.6 %	336 \pm 259	148 \pm 195	20.6 \pm 18.7	71.0 \pm 133	
	Propene (pptV)	6.9 %	8.6 \pm 8.6	8.8 \pm 11.5	8.0 \pm 6.2	7.2 \pm 6.1	
	Iso-butane (pptV)	6.4 %	40.4 \pm 39.5	11.0 \pm 20.0	3.2 \pm 4.3	8.4 \pm 15.5	R. Steinbrecher (2019)
	n-butane (pptV)	5.0 %	82.8 \pm 80.7	19.4 \pm 36.0	6.0 \pm 7.3	22.1 \pm 40.5	
	Iso-pentane (pptV)	4.6 %	11.1 \pm 14.9	3.6 \pm 6.2	5.2 \pm 9.5	4.0 \pm 6.7	
	n-pentane (pptV)	6.4 %	8.7 \pm 11.4	2.9 \pm 4.7	1.7 \pm 2.6	3.5 \pm 5.2	
	Benzene (pptV)	4.8 %	40.1 \pm 30.5	22.9 \pm 23.3	11.1 \pm 10.5	17.3 \pm 11.5	
	Toluene (pptV)	6.3 %	4.6 \pm 5.4	3.0 \pm 4.2	2.9 \pm 2.8	3.4 \pm 3.1	
	Methanol (pptV)	20.7 %	486 \pm 563	698 \pm 734	677 \pm 603	857 \pm 655	
	Acetone (pptV)	12.2 %	506 \pm 263	614 \pm 274	767 \pm 332	681 \pm 213	
Campbell Scientific weather station	Temperature (°C)	0.4 °C at 5-40 °C	22.0 \pm 2.3	21.7 \pm 1.4	24.5 \pm 2.5	25.8 \pm 2.1	
	Pressure (hPa)	1.0 hPa at 0-40°C	1016 \pm 4	1016 \pm 3	1015 \pm 4	1014 \pm 3	Carpenter et al. (2010)
	Relative Humidity (%)	2 % at 10-90 %	74.9 \pm 12.8	77.2 \pm 10.4	82.8 \pm 8.8	81.1 \pm 11.9	
	Solar Radiation (W m ⁻²)	5%	615 \pm 312	785 \pm 251	737 \pm 283	716 \pm 273	

674 ^aMidday (12.00-15.00 UTC, local +1) mean $\pm 2\sigma$ for July 2017 – June 2020. ^bFor further
675 information on the instrument and the data processing. ^cAverage uncertainties determined as
676 described in Andersen et al. (2021). ^dPercentage given is relevant to average midday
677 uncertainty. ^eEstimated from zero measurements and from running two O₃ instruments
678 together.

Table 3: Potential sources of NO₂ artefacts at the CVAO.

	ACS at 380 nm (10 ⁻²⁰ cm ²) ^a	ACS at 385 nm (10 ⁻²⁰ cm ²) ^a	ACS at 390 nm (10 ⁻²⁰ cm ²) ^a	Conversion efficiency (%) ^b	Measured at the CVAO at midday (pptV) ^c	Modelled by GEOS Chem at midday (pptV) ^c	Potential artefact (pptV)
NO ₂ → NO ^{hv}	59.24	59.42	62.0	50	-	-	-
BrONO ₂ → NO ₂ ^{hv}	3.85	3.37	2.97	2.8	-	0.5-1.5	0.014-0.042
ClONO ₂ → NO ₂ ^{hv}	0.121	0.137	0.091	0.1	-	0.5-1	0.0005-0.001
ClNO → NO ^{hv}	8.86	7.82	6.86	6.6	-	-	-
ClNO ₂ → NO ₂ ^{hv}	0.3593	0.2687	0.2008	0.2	-	~0	-
BrNO ₂ → NO ₂ ^{hv}	17	17	16	14.3	-	~0	-
HONO → NO ^{hv}	9.2	14.5	2.4	6.3	3-5	0.2-0.4	0.38-0.63
PAN ^Δ → NO ₂	-	-	-	~5	< 6	~20	< 0.28
Total	-	-	-	-	-	-	0.67-0.95

^aAll absorption cross sections have been reported by IUPAC (Atkinson et al., 2004). ^bThe reported conversion efficiencies have been calculated based on a NO₂ CE of 50%. ^cMidday is defined as 12.00-15.00 UTC (local+1).

Table 4: Summary over the required additional artefact, RO₂, and XO to give [NO₂]_{obs./[NO₂]_{PSS ext.} = 1 given as 50th (25th-75th) percentile when subtracting a NO₂ artefact of 0.7 pptV.}

	[CO] < 90 ppbV	90 ppbV < [CO] < 100 ppbV	[CO] > 100 ppbV
$\frac{[\text{NO}_2]_{\text{obs.}}}{[\text{NO}_2]_{\text{PSS ext.}}}$	1.00 (0.76 - 1.29)	1.14 (0.89 - 1.47)	1.42 (1.12 - 1.68)
Required additional artefact (pptV)	0.00 (-2.65 - 1.70)	1.9 (0.92 - 5.27)	4.4 (0.95 - 9.27)
Case I: Using BrO = 2.5 pptV and IO = 1.4 pptV			
Required RO _x (pptV) ^a	49.45 (16.18 - 87.63)	65.0 (33.68 - 112.5)	109.7 (63.14 - 149.5)
Modelled RO _x (pptV)	48.89 (46.01 - 53.35)	45.60 (35.69 - 54.71)	44.99 (37.31 - 54.70)
Required RO ₂ (pptV) ^b	31.77 (-1.79 - 69.99)	47.53 (16.81 - 93.93)	90.49 (45.04 - 128.5)
Modelled RO ₂ (pptV)	33.66 (30.07 - 34.43)	29.89 (21.50 - 36.32)	27.62 (20.93 - 35.42)
Missing RO ₂ (pptV) ^c	-0.25 (-31.85 - 39.69)	20.19 (-14.23 - 66.44)	61.33 (18.53 - 104.3)
Case II: Using modelled RO₂ and HO₂			
Required XO (pptV) ^d	3.72 (-7.94 - 18.55)	11.31 (-1.46 - 28.46)	26.58 (10.70 - 42.52)
Missing XO (pptV) ^e	-0.18 (-11.84 - 14.65)	7.41 (-5.36 - 24.56)	22.68 (6.80 - 38.62)

^aCalculated using equation (IV). ^bCalculated using equation (VIII). ^cCalculated using equation (IX). ^dCalculated using equation (V). ^eSubtracted 3.9 pptV of XO from the required XO (2.5 pptV BrO + 1.4 pptV IO).

11 References

- 685 Andersen, S. T., Carpenter, L. J., Nelson, B. S., Neves, L., Read, K. A., Reed, C., Ward, M.,
Rowlinson, M. J., and Lee, J. D.: Long-term NO_x measurements in the remote marine
tropical troposphere, *Atmos. Meas. Tech.*, 14, 3071-3085, 10.5194/amt-14-3071-2021,
2021.
- 690 Atkinson, R., Baulch, D. L., Cox, R. A., Crowley, J. N., Hampson, R. F., Hynes, R. G., Jenkin,
M. E., Rossi, M. J., and Troe, J.: IUPAC Task Group on Atmospheric Chemical Kinetic
Data Evaluation, *Atmos. Chem. Phys.*, 4, 2004.
- Atkinson, R., Baulch, D. L., Cox, R. A., Crowley, J. N., Hampson, R. F., Hynes, R. G., Jenkin,
M. E., Rossi, M. J., Troe, J., and Subcommittee, I.: Evaluated kinetic and photochemical
data for atmospheric chemistry: Volume II; gas phase reactions of organic species, *Atmos.*
Chem. Phys., 6, 3625-4055, 10.5194/acp-6-3625-2006, 2006.
- 695 Ayers, G. P., Penkett, S. A., Gillett, R. W., Bandy, B., Galbally, I. E., Meyer, C. P., Elsworth,
C. M., Bentley, S. T., and Forgan, B. W.: Evidence for photochemical control of ozone
concentrations in unpolluted marine air, *Nature*, 360, 446-449, 10.1038/360446a0, 1992.
- Ayers, G. P., and Galbally, I. E.: A preliminary investigation of a boundary layer-free
troposphere entrainment velocity at Cape Grim, *Baseline* 92, 1995.
- 700 Bloss, W. J., Evans, M. J., Lee, J. D., Sommariva, R., Heard, D. E., and Pilling, M. J.: The
oxidative capacity of the troposphere: Coupling of field measurements of OH and a global
chemistry transport model, *Faraday Discussions*, 130, 425-436, 10.1039/B419090D, 2005.
- Bradshaw, J., Davis, D., Crawford, J., Chen, G., Shetter, R., Müller, M., Gregory, G., Sachse,
G., Blake, D., Heikes, B., Singh, H., Mastromarino, J., and Sandholm, S.:
705 Photofragmentation two-photon laser-induced fluorescence detection of NO₂ and NO:
Comparison of measurements with model results based on airborne observations during
PEM-Tropics A, *Geophysical Research Letters*, 26, 471-474,
<https://doi.org/10.1029/1999GL900015>, 1999.
- Bridier, I., Caralp, F., Loirat, H., Lesclaux, R., Veyret, B., Becker, K. H., Reimer, A., and
710 Zabel, F.: Kinetic and theoretical studies of the reactions acetylperoxy + nitrogen dioxide
+ M \rightleftharpoons acetyl peroxyxynitrate + M between 248 and 393 K and between 30 and 760 torr, *The
Journal of Physical Chemistry*, 95, 3594-3600, 10.1021/j100162a031, 1991.
- Burkert, J., Andrés-Hernández, M.-D., Stöbener, D., Burrows, J. P., Weissenmayer, M., and
715 Kraus, A.: Peroxy radical and related trace gas measurements in the boundary layer above
the Atlantic Ocean, *Journal of Geophysical Research: Atmospheres*, 106, 5457-5477,
<https://doi.org/10.1029/2000JD900613>, 2001.
- Butkovskaya, N., Kukui, A., and Le Bras, G.: HNO₃ Forming Channel of the HO₂ + NO
Reaction as a Function of Pressure and Temperature in the Ranges of 72–600 Torr and
223–323 K, *The Journal of Physical Chemistry A*, 111, 9047-9053, 10.1021/jp074117m,
720 2007.
- Butkovskaya, N., Rayez, M.-T., Rayez, J.-C., Kukui, A., and Le Bras, G.: Water Vapor Effect
on the HNO₃ Yield in the HO₂ + NO Reaction: Experimental and Theoretical Evidence,
The Journal of Physical Chemistry A, 113, 11327-11342, 10.1021/jp811428p, 2009.
- 725 Calvert, J. G., and Stockwell, W. R.: Deviations from the O₃–NO–NO₂ photostationary state
in tropospheric chemistry, *Canadian Journal of Chemistry*, 61, 983-992, 10.1139/v83-174,
1983.
- Cantrell, C. A., Lind, J. A., Shetter, R. E., Calvert, J. G., Goldan, P. D., Kuster, W., Fehsenfeld,
F. C., Montzka, S. A., Parrish, D. D., Williams, E. J., Buhr, M. P., Westberg, H. H.,
Allwine, G., and Martin, R.: Peroxy radicals in the ROSE experiment: Measurement and
730 theory, *Journal of Geophysical Research: Atmospheres*, 97, 20671-20686,
<https://doi.org/10.1029/92JD01727>, 1992.

- 735 Cantrell, C. A., Shetter, R. E., Calvert, J. G., Parrish, D. D., Fehsenfeld, F. C., Goldan, P. D.,
Kuster, W., Williams, E. J., Westberg, H. H., Allwine, G., and Martin, R.: Peroxy radicals
as measured in ROSE and estimated from photostationary state deviations, *Journal of
Geophysical Research: Atmospheres*, 98, 18355-18366,
<https://doi.org/10.1029/93JD01794>, 1993a.
- 740 Cantrell, C. A., Shetter, R. E., Lind, J. A., McDaniel, A. H., Calvert, J. G., Parrish, D. D.,
Fehsenfeld, F. C., Buhr, M. P., and Trainer, M.: An improved chemical amplifier technique
for peroxy radical measurements, *Journal of Geophysical Research: Atmospheres*, 98,
2897-2909, <https://doi.org/10.1029/92JD02842>, 1993b.
- Cantrell, C. A., Shetter, R. E., Gilpin, T. M., and Calvert, J. G.: Peroxy radicals measured
during Mauna Loa Observatory Photochemistry Experiment 2: The data and first analysis,
Journal of Geophysical Research: Atmospheres, 101, 14643-14652,
<https://doi.org/10.1029/95JD01698>, 1996.
- 745 Cantrell, C. A., Shetter, R. E., Calvert, J. G., Eisele, F. L., Williams, E., Baumann, K., Brune,
W. H., Stevens, P. S., and Mather, J. H.: Peroxy radicals from photostationary state
deviations and steady state calculations during the Tropospheric OH Photochemistry
Experiment at Idaho Hill, Colorado, 1993, *Journal of Geophysical Research: Atmospheres*,
102, 6369-6378, <https://doi.org/10.1029/96JD01703>, 1997.
- 750 Carpenter, L. J., Monks, P. S., Bandy, B. J., Penkett, S. A., Galbally, I. E., and Meyer, C. P.: A
study of peroxy radicals and ozone photochemistry at coastal sites in the northern and
southern hemispheres, *Journal of Geophysical Research: Atmospheres*, 102, 25417-25427,
<https://doi.org/10.1029/97JD02242>, 1997.
- 755 Carpenter, L. J., Clemitshaw, K. C., Burgess, R. A., Penkett, S. A., Cape, J. N., and McFadyen,
G. G.: Investigation and evaluation of the NO_x/O₃ photochemical steady state,
Atmospheric Environment, 32, 3353-3365, [https://doi.org/10.1016/S1352-
2310\(97\)00416-0](https://doi.org/10.1016/S1352-2310(97)00416-0), 1998.
- 760 Carpenter, L. J., Fleming, Z. L., Read, K. A., Lee, J. D., Moller, S. J., Hopkins, J. R., Purvis,
R. M., Lewis, A. C., Müller, K., Heinold, B., Herrmann, H., Fomba, K. W., van Pinxteren,
D., Müller, C., Tegen, I., Wiedensohler, A., Müller, T., Niedermeier, N., Achterberg, E.
P., Patey, M. D., Kozlova, E. A., Heimann, M., Heard, D. E., Plane, J. M. C., Mahajan, A.,
Oetjen, H., Ingham, T., Stone, D., Whalley, L. K., Evans, M. J., Pilling, M. J., Leigh, R.
J., Monks, P. S., Karunaharan, A., Vaughan, S., Arnold, S. R., Tschirner, J., Pöhler, D.,
765 Frieß, U., Holla, R., Mendes, L. M., Lopez, H., Faria, B., Manning, A. J., and Wallace, D.
W. R.: Seasonal characteristics of tropical marine boundary layer air measured at the Cape
Verde Atmospheric Observatory, *Journal of Atmospheric Chemistry*, 67, 87-140,
[10.1007/s10874-011-9206-1](https://doi.org/10.1007/s10874-011-9206-1), 2010.
- 770 Carsey, T. P., Churchill, D. D., Farmer, M. L., Fischer, C. J., Pszenny, A. A., Ross, V. B.,
Saltzman, E. S., Springer-Young, M., and Bonsang, B.: Nitrogen oxides and ozone
production in the North Atlantic marine boundary layer, *Journal of Geophysical Research:
Atmospheres*, 102, 10653-10665, [10.1029/96JD03511](https://doi.org/10.1029/96JD03511), 1997.
- 775 Clemitshaw, K. C., Carpenter, L. J., Penkett, S. A., and Jenkin, M. E.: A calibrated peroxy
radical chemical amplifier for ground-based tropospheric measurements, *Journal of
Geophysical Research: Atmospheres*, 102, 25405-25416,
<https://doi.org/10.1029/97JD01902>, 1997.
- Cox, R. A.: Ozone and peroxy radical budgets in the marine boundary layer: Modeling the
effect of NO_x, *Journal of Geophysical Research: Atmospheres*, 104, 8047-8056,
<https://doi.org/10.1029/1998JD100104>, 1999.
- 780 Crawford, J., Davis, D., Chen, G., Bradshaw, J., Sandholm, S., Gregory, G., Sachse, G.,
Anderson, B., Collins, J., Blake, D., Singh, H., Heikes, B., Talbot, R., and Rodriguez, J.:
Photostationary state analysis of the NO₂-NO system based on airborne observations from

- the western and central North Pacific, *Journal of Geophysical Research: Atmospheres*, 101, 2053-2072, <https://doi.org/10.1029/95JD02201>, 1996.
- 785 Duncianu, M., Lahib, A., Tomas, A., Stevens, P. S., and Dusanter, S.: Characterization of a chemical amplifier for peroxy radical measurements in the atmosphere, *Atmospheric Environment*, 222, 117106, <https://doi.org/10.1016/j.atmosenv.2019.117106>, 2020.
- Emmerson, K. M., Carslaw, N., Carslaw, D. C., Lee, J. D., McFiggans, G., Bloss, W. J., Gravestock, T., Heard, D. E., Hopkins, J., Ingham, T., Pilling, M. J., Smith, S. C., Jacob, M., and Monks, P. S.: Free radical modelling studies during the UK TORCH Campaign in Summer 2003, *Atmos. Chem. Phys.*, 7, 167-181, 10.5194/acp-7-167-2007, 2007.
- 790 Fairlie, T. D., Jacob, D. J., Dibb, J. E., Alexander, B., Avery, M. A., van Donkelaar, A., and Zhang, L.: Impact of mineral dust on nitrate, sulfate, and ozone in transpacific Asian pollution plumes, *Atmos. Chem. Phys.*, 10, 3999-4012, 10.5194/acp-10-3999-2010, 2010.
- 795 Gao, R. S., Keim, E. R., Woodbridge, E. L., Ciciora, S. J., Proffitt, M. H., Thompson, T. L., Mclaughlin, R. J., and Fahey, D. W.: New photolysis system for NO₂ measurements in the lower stratosphere, *Journal of Geophysical Research: Atmospheres*, 99, 20673-20681, <https://doi.org/10.1029/94JD01521>, 1994.
- Handisides, G. M., Plass-Dülmer, C., Gilge, S., Bingemer, H., and Berresheim, H.: Hohenpeissenberg Photochemical Experiment (HOPE 2000): Measurements and photostationary state calculations of OH and peroxy radicals, *Atmos. Chem. Phys.*, 3, 1565-1588, 10.5194/acp-3-1565-2003, 2003.
- 800 Hauglustaine, D. A., Madronich, S., Ridley, B. A., Walega, J. G., Cantrell, C. A., Shetter, R. E., and Hübler, G.: Observed and model-calculated photostationary state at Mauna Loa Observatory during MLOPEX 2, *Journal of Geophysical Research: Atmospheres*, 101, 14681-14696, <https://doi.org/10.1029/95JD03612>, 1996.
- 805 Hauglustaine, D. A., Madronich, S., Ridley, B. A., Flocke, S. J., Cantrell, C. A., Eisele, F. L., Shetter, R. E., Tanner, D. J., Ginoux, P., and Atlas, E. L.: Photochemistry and budget of ozone during the Mauna Loa Observatory Photochemistry Experiment (MLOPEX 2), *Journal of Geophysical Research: Atmospheres*, 104, 30275-30307, <https://doi.org/10.1029/1999JD900441>, 1999.
- 810 Hernández, M. D. A., Burkert, J., Reichert, L., Stöbener, D., Meyer-Arne, J., Burrows, J. P., Dickerson, R. R., and Doddridge, B. G.: Marine boundary layer peroxy radical chemistry during the AEROSOLS99 campaign: Measurements and analysis, *Journal of Geophysical Research: Atmospheres*, 106, 20833-20846, <https://doi.org/10.1029/2001JD900113>, 2001.
- 815 Hosaynali Beygi, Z., Fischer, H., Harder, H. D., Martinez, M., Sander, R., Williams, J., Brookes, D. M., Monks, P. S., and Lelieveld, J.: Oxidation photochemistry in the Southern Atlantic boundary layer: unexpected deviations of photochemical steady state, *Atmos. Chem. Phys.*, 11, 8497-8513, 10.5194/acp-11-8497-2011, 2011.
- 820 Inamdar, S., Tinel, L., Chance, R., Carpenter, L. J., Sabu, P., Chacko, R., Tripathy, S. C., Kerkar, A. U., Sinha, A. K., Bhaskar, P. V., Sarkar, A., Roy, R., Sherwen, T., Cuevas, C., Saiz-Lopez, A., Ram, K., and Mahajan, A. S.: Estimation of reactive inorganic iodine fluxes in the Indian and Southern Ocean marine boundary layer, *Atmos. Chem. Phys.*, 20, 12093-12114, 10.5194/acp-20-12093-2020, 2020.
- 825 Jacob, D. J., Heikes, E. G., Fan, S.-M., Logan, J. A., Mauzerall, D. L., Bradshaw, J. D., Singh, H. B., Gregory, G. L., Talbot, R. W., Blake, D. R., and Sachse, G. W.: Origin of ozone and NO_x in the tropical troposphere: A photochemical analysis of aircraft observations over the South Atlantic basin, 101, 24235-24250, doi:10.1029/96JD00336, 1996.
- Jenkin, M. E., Young, J. C., and Rickard, A. R.: The MCM v3.3.1 degradation scheme for isoprene, *Atmos. Chem. Phys.*, 15, 11433-11459, 10.5194/acp-15-11433-2015, 2015.
- 830 Kleindienst, T. E.: Recent developments in the chemistry and biology of peroxyacetyl nitrate, *Research on Chemical Intermediates*, 20, 335-384, 10.1163/156856794X00379, 1994.

- 835 Lee, J. D., Moller, S. J., Read, K. A., Lewis, A. C., Mendes, L., and Carpenter, L. J.: Year-round measurements of nitrogen oxides and ozone in the tropical North Atlantic marine boundary layer, *Journal of Geophysical Research: Atmospheres*, 114, <https://doi.org/10.1029/2009JD011878>, 2009.
- Leighton, P. A.: *Photochemistry of Air Pollution*, Academic Press, 1961.
- Liu, Y., and Zhang, J.: Atmospheric Peroxy Radical Measurements Using Dual-Channel Chemical Amplification Cavity Ringdown Spectroscopy, *Analytical chemistry*, 86, 5391-5398, 10.1021/ac5004689, 2014.
- 840 Ma, Y., Lu, K., Chou, C. C. K., Li, X., and Zhang, Y.: Strong deviations from the NO-NO₂-O₃ photostationary state in the Pearl River Delta: Indications of active peroxy radical and chlorine radical chemistry, *Atmospheric Environment*, 163, 22-34, <https://doi.org/10.1016/j.atmosenv.2017.05.012>, 2017.
- 845 Mahajan, A. S., Plane, J. M. C., Oetjen, H., Mendes, L., Saunders, R. W., Saiz-Lopez, A., Jones, C. E., Carpenter, L. J., and McFiggans, G. B.: Measurement and modelling of tropospheric reactive halogen species over the tropical Atlantic Ocean, *Atmos. Chem. Phys.*, 10, 4611-4624, 10.5194/acp-10-4611-2010, 2010.
- 850 Mahajan, A. S., Whalley, L. K., Kozlova, E., Oetjen, H., Mendez, L., Furneaux, K. L., Goddard, A., Heard, D. E., Plane, J. M. C., and Saiz-Lopez, A.: DOAS observations of formaldehyde and its impact on the HO_x balance in the tropical Atlantic marine boundary layer, *Journal of Atmospheric Chemistry*, 66, 167, 10.1007/s10874-011-9200-7, 2011.
- 855 Mannschreck, K., Gilge, S., Plass-Duelmer, C., Fricke, W., and Berresheim, H.: Assessment of the applicability of NO-NO₂-O₃ photostationary state to long-term measurements at the Hohenpeissenberg GAW Station, Germany, *Atmos. Chem. Phys.*, 4, 1265-1277, 10.5194/acp-4-1265-2004, 2004.
- Mihele, C. M., and Hastie, D. R.: The sensitivity of the radical amplifier to ambient water vapour, *Geophysical Research Letters*, 25, 1911-1913, <https://doi.org/10.1029/98GL01432>, 1998.
- 860 Miyazaki, K., Parker, A. E., Fittschen, C., Monks, P. S., and Kajii, Y.: A new technique for the selective measurement of atmospheric peroxy radical concentrations of HO₂ and RO₂ using a denuding method, *Atmos. Meas. Tech.*, 3, 1547-1554, 10.5194/amt-3-1547-2010, 2010.
- 865 Parrish, D. D., Trainer, M., Williams, E. J., Fahey, D. W., Hübler, G., Eubank, C. S., Liu, S. C., Murphy, P. C., Albritton, D. L., and Fehsenfeld, F. C.: Measurements of the NO_x-O₃ photostationary state at Niwot Ridge, Colorado, *Journal of Geophysical Research: Atmospheres*, 91, 5361-5370, <https://doi.org/10.1029/JD091iD05p05361>, 1986.
- 870 Parrish, D. D., Hahn, C. H., Fahey, D. W., Williams, E. J., Bollinger, M. J., Hübler, G., Buhr, M. P., Murphy, P. C., Trainer, M., Hsie, E. Y., Liu, S. C., and Fehsenfeld, F. C.: Systematic variations in the concentration of NO_x (NO + NO₂) at Niwot Ridge, Colorado, *Journal of Geophysical Research: Atmospheres*, 95, 1817-1836, <https://doi.org/10.1029/JD095iD02p01817>, 1990.
- Peterson, M. C., and Honrath, R. E.: NO_x and NO_y over the northwestern North Atlantic: Measurements and measurement accuracy, *Journal of Geophysical Research: Atmospheres*, 104, 11695-11707, 1999.
- 875 Pinto, J. P., Dibb, J., Lee, B. H., Rappenglück, B., Wood, E. C., Levy, M., Zhang, R.-Y., Lefer, B., Ren, X.-R., Stutz, J., Tsai, C., Ackermann, L., Golovko, J., Herndon, S. C., Oakes, M., Meng, Q.-Y., Munger, J. W., Zahniser, M., and Zheng, J.: Intercomparison of field measurements of nitrous acid (HONO) during the SHARP campaign, *Journal of Geophysical Research: Atmospheres*, 119, 5583-5601, <https://doi.org/10.1002/2013JD020287>, 2014.
- 880

- Pollack, I. B., Lerner, B. M., and Ryerson, T. B.: Evaluation of ultraviolet light-emitting diodes for detection of atmospheric NO₂ by photolysis - chemiluminescence, *Journal of Atmospheric Chemistry*, 65, 111-125, 10.1007/s10874-011-9184-3, 2010.
- 885 Prados-Roman, C., Cuevas, C. A., Hay, T., Fernandez, R. P., Mahajan, A. S., Royer, S. J., Galí, M., Simó, R., Dachs, J., Großmann, K., Kinnison, D. E., Lamarque, J. F., and Saiz-Lopez, A.: Iodine oxide in the global marine boundary layer, *Atmos. Chem. Phys.*, 15, 583-593, 10.5194/acp-15-583-2015, 2015.
- 890 Read, K. A., Mahajan, A. S., Carpenter, L. J., Evans, M. J., Faria, B. V. E., Heard, D. E., Hopkins, J. R., Lee, J. D., Moller, S. J., Lewis, A. C., Mendes, L., McQuaid, J. B., Oetjen, H., Saiz-Lopez, A., Pilling, M. J., and Plane, J. M. C.: Extensive halogen-mediated ozone destruction over the tropical Atlantic Ocean, *Nature*, 453, 1232, 10.1038/nature07035
- <https://www.nature.com/articles/nature07035#supplementary-information>, 2008.
- 895 Read, K. A., Lee, J. D., Lewis, A. C., Moller, S. J., Mendes, L., and Carpenter, L. J.: Intra-annual cycles of NMVOC in the tropical marine boundary layer and their use for interpreting seasonal variability in CO, *Journal of Geophysical Research: Atmospheres*, 114, <https://doi.org/10.1029/2009JD011879>, 2009.
- Reed, C., Evans, M. J., Carlo, P. D., Lee, J. D., and Carpenter, L. J.: Interferences in photolytic NO₂ measurements: explanation for an apparent missing oxidant?, *Atmospheric Chemistry Physics*, 16, 4707-4724, 2016.
- 900 Reed, C., Evans, M. J., Crilley, L. R., Bloss, W. J., Sherwen, T., Read, K. A., Lee, J. D., and Carpenter, L. J.: Evidence for renoxification in the tropical marine boundary layer, *Atmos. Chem. Phys.*, 17, 4081-4092, 10.5194/acp-17-4081-2017, 2017.
- Rhoads, K. P., Kelley, P., Dickerson, R. R., Carsey, T. P., Farmer, M., Savoie, D. L., and Prospero, J. M.: Composition of the troposphere over the Indian Ocean during the monsoonal transition, *Journal of Geophysical Research: Atmospheres*, 102, 18981-18995, 10.1029/97JD01078, 1997.
- 905 Ridley, B. A., Carroll, M. A., Gregory, G. L., and Sachse, G. W.: NO and NO₂ in the troposphere: Technique and measurements in regions of a folded tropopause, *Journal of Geophysical Research: Atmospheres*, 93, 15813-15830, <https://doi.org/10.1029/JD093iD12p15813>, 1988.
- 910 Ridley, B. A., Madronich, S., Chatfield, R. B., Walega, J. G., Shetter, R. E., Carroll, M. A., and Montzka, D. D.: Measurements and model simulations of the photostationary state during the Mauna Loa Observatory Photochemistry Experiment: Implications for radical concentrations and ozone production and loss rates, *Journal of Geophysical Research: Atmospheres*, 97, 10375-10388, <https://doi.org/10.1029/91JD02287>, 1992.
- 915 Ryerson, T. B., Williams, E. J., and Fehsenfeld, F. C.: An efficient photolysis system for fast-response NO₂ measurements, *Journal of Geophysical Research: Atmospheres*, 105, 26447-26461, 10.1029/2000jd900389, 2000.
- 920 Sadanaga, Y., Matsumoto, J., Sakurai, K.-i., Isozaki, R., Kato, S., Nomaguchi, T., Bandow, H., and Kajii, Y.: Development of a measurement system of peroxy radicals using a chemical amplification/laser-induced fluorescence technique, *Review of Scientific Instruments*, 75, 864-872, 10.1063/1.1666985, 2004.
- Saiz-Lopez, A., Plane, J. M. C., Baker, A. R., Carpenter, L. J., von Glasow, R., Gómez Martín, J. C., McFiggans, G., and Saunders, R. W.: Atmospheric Chemistry of Iodine, *Chemical Reviews*, 112, 1773-1804, 10.1021/cr200029u, 2012.
- 925 Sherwen, T., Evans, M. J., Carpenter, L. J., Andrews, S. J., Lidster, R. T., Dix, B., Koenig, T. K., Sinreich, R., Ortega, I., Volkamer, R., Saiz-Lopez, A., Prados-Roman, C., Mahajan, A. S., and Ordóñez, C.: Iodine's impact on tropospheric oxidants: a global model study in GEOS-Chem, *Atmos. Chem. Phys.*, 16, 1161-1186, 10.5194/acp-16-1161-2016, 2016.

- 930 Sillman, S.: The relation between ozone, NO_x and hydrocarbons in urban and polluted rural environments, *Atmospheric Environment*, 33, 1821-1845, [https://doi.org/10.1016/S1352-2310\(98\)00345-8](https://doi.org/10.1016/S1352-2310(98)00345-8), 1999.
- Sommariva, R., Cox, S., Martin, C., Borońska, K., Young, J., Jimack, P. K., Pilling, M. J., Matthaios, V. N., Nelson, B. S., Newland, M. J., Panagi, M., Bloss, W. J., Monks, P. S.,
935 and Rickard, A. R.: AtChem (version 1), an open-source box model for the Master Chemical Mechanism, *Geosci. Model Dev.*, 13, 169-183, 10.5194/gmd-13-169-2020, 2020.
- Steinbrecher, R.: SYSTEM AND PERFORMANCE AUDIT FOR NON METHANE VOLATILE ORGANIC COMPOUNDS: Global GAW Station – Cape Verde Atmospheric Observatory Calhau, Cape Verde, WMO World Calibration Centre for VOC, Karlsruhe Institute of Technology, KIT/IMK-IFU, Garmisch-Partenkirchen, Germany,
940 2019.
- Syomin, D. A., and Finlayson-Pitts, B. J.: HONO decomposition on borosilicate glass surfaces: implications for environmental chamber studies and field experiments, *Physical Chemistry Chemical Physics*, 5, 5236-5242, 10.1039/B309851F, 2003.
945
- Tadic, I., Crowley, J. N., Dienhart, D., Eger, P., Harder, H., Hottmann, B., Martinez, M., Parchatka, U., Paris, J. D., Pozzer, A., Rohloff, R., Schuladen, J., Shenolikar, J., Tauer, S., Lelieveld, J., and Fischer, H.: Net ozone production and its relationship to nitrogen oxides and volatile organic compounds in the marine boundary layer around the Arabian Peninsula, *Atmos. Chem. Phys.*, 20, 6769-6787, 10.5194/acp-20-6769-2020, 2020.
950
- Trebs, I., Mayol-Bracero, O. L., Pauliquevis, T., Kuhn, U., Sander, R., Ganzeveld, L., Meixner, F. X., Kesselmeier, J., Artaxo, P., and Andreae, M. O.: Impact of the Manaus urban plume on trace gas mixing ratios near the surface in the Amazon Basin: Implications for the NO-NO₂-O₃ photostationary state and peroxy radical levels, *Journal of Geophysical Research: Atmospheres*, 117, <https://doi.org/10.1029/2011JD016386>, 2012.
955
- Vaughan, S., Ingham, T., Whalley, L. K., Stone, D., Evans, M. J., Read, K. A., Lee, J. D., Moller, S. J., Carpenter, L. J., Lewis, A. C., Fleming, Z. L., and Heard, D. E.: Seasonal observations of OH and HO₂ in the remote tropical marine boundary layer, *Atmos. Chem. Phys.*, 12, 2149-2172, 10.5194/acp-12-2149-2012, 2012.
- 960 Vogt, R., Sander, R., von Glasow, R., and Crutzen, P. J.: Iodine Chemistry and its Role in Halogen Activation and Ozone Loss in the Marine Boundary Layer: A Model Study, *Journal of Atmospheric Chemistry*, 32, 375-395, 10.1023/A:1006179901037, 1999.
- Volz-Thomas, A., Pätz, H.-W., Houben, N., Konrad, S., Mihelcic, D., Klüpfel, T., and Perner, D.: Inorganic trace gases and peroxy radicals during BERLIOZ at Pabstthum: An investigation of the photostationary state of NO_x and O₃, *Journal of Geophysical Research: Atmospheres*, 108, PHO 4-1-PHO 4-15, <https://doi.org/10.1029/2001JD001255>, 2003.
965
- Wang, X., Jacob, D. J., Downs, W., Zhai, S., Zhu, L., Shah, V., Holmes, C. D., Sherwen, T., Alexander, B., Evans, M. J., Eastham, S. D., Neuman, J. A., Veres, P. R., Koenig, T. K., Volkamer, R., Huey, L. G., Bannan, T. J., Percival, C. J., Lee, B. H., and Thornton, J. A.:
970 Global tropospheric halogen (Cl, Br, I) chemistry and its impact on oxidants, *Atmos. Chem. Phys.*, 21, 13973-13996, 10.5194/acp-21-13973-2021, 2021.
- Whalley, L. K., Lewis, A. C., McQuaid, J. B., Purvis, R. M., Lee, J. D., Stemmler, K., Zellweger, C., and Ridgeon, P.: Two high-speed, portable GC systems designed for the measurement of non-methane hydrocarbons and PAN: Results from the Jungfraujoch High Altitude Observatory, *Journal of Environmental Monitoring*, 6, 234-241, 10.1039/B310022G, 2004.
975
- Whalley, L. K., Furneaux, K. L., Goddard, A., Lee, J. D., Mahajan, A., Oetjen, H., Read, K. A., Kaaden, N., Carpenter, L. J., Lewis, A. C., Plane, J. M. C., Saltzman, E. S., Wiedensohler, A., and Heard, D. E.: The chemistry of OH and HO₂ radicals in the

- 980 boundary layer over the tropical Atlantic Ocean, *Atmos. Chem. Phys.*, 10, 1555-1576, 10.5194/acp-10-1555-2010, 2010.
- Williams, E. J., Roberts, J. M., Baumann, K., Bertman, S. B., Buhr, S., Norton, R. B., and Fehsenfeld, F. C.: Variations in NO_y composition at Idaho Hill, Colorado, *Journal of Geophysical Research: Atmospheres*, 102, 6297-6314, 985 <https://doi.org/10.1029/96JD03252>, 1997.
- Wofsy, S. C., Afshar, S., Allen, H. M., Apel, E. C., Asher, E. C., Barletta, B., Bent, J., Bian, H., Biggs, B. C., Blake, D. R., Blake, N., Bourgeois, I., Brock, C. A., Brune, W. H., Budney, J. W., Bui, T. P., Butler, A., Campuzano-Jost, P., Chang, C. S., Chin, M., Commane, R., Correa, G., Crouse, J. D., Cullis, P. D., Daube, B. C., Day, D. A., Dean-Day, J. M., Dibb, J. E., DiGangi, J. P., Diskin, G. S., Dollner, M., Elkins, J. W., Erdesz, F., Fiore, A. M., Flynn, C. M., Froyd, K. D., Gesler, D. W., Hall, S. R., Hanisco, T. F., Hannun, R. A., Hills, A. J., Hintsa, E. J., Hoffman, A., Hornbrook, R. S., Huey, L. G., Hughes, S., Jimenez, J. L., Johnson, B. J., Katich, J. M., Keeling, R. F., Kim, M. J., Kupc, A., Lait, L. R., McKain, K., McLaughlin, R. J., Meinardi, S., Miller, D. O., Montzka, S. A., Moore, F. L., Morgan, E. J., Murphy, D. M., Murray, L. T., Nault, B. A., Neuman, J. A., Newman, P. A., Nicely, J. M., Pan, X., Paplawsky, W., Peischl, J., Prather, M. J., Price, D. J., Ray, E. A., Reeves, J. M., Richardson, M., Rollins, A. W., Rosenlof, K. H., Ryerson, T. B., Scheuer, E., Schill, G. P., Schroder, J. C., Schwarz, J. P., St.Clair, J. M., Steenrod, S. D., Stephens, B. B., Strode, S. A., Sweeney, C., Tanner, D., Teng, A. P., Thames, A. B., Thompson, C. R., Ullmann, K., Veres, P. R., Wagner, N. L., Watt, A., Weber, R., Weinzierl, B. B., Wennberg, P. O., Williamson, C. J., Wilson, J. C., Wolfe, G. M., Woods, C. T., Zeng, L. H., and Vieznor, N.: ATom: Merged Atmospheric Chemistry, Trace Gases, and Aerosols, Version 2, in, ORNL Distributed Active Archive Center, 2021.
- 1000 Wolfe, G. M., Cantrell, C., Kim, S., Mauldin Iii, R. L., Karl, T., Harley, P., Turnipseed, A., Zheng, W., Flocke, F., Apel, E. C., Hornbrook, R. S., Hall, S. R., Ullmann, K., Henry, S. B., DiGangi, J. P., Boyle, E. S., Kaser, L., Schnitzhofer, R., Hansel, A., Graus, M., Nakashima, Y., Kajii, Y., Guenther, A., and Keutsch, F. N.: Missing peroxy radical sources within a summertime ponderosa pine forest, *Atmos. Chem. Phys.*, 14, 4715-4732, 10.5194/acp-14-4715-2014, 2014.
- 1005
- 1010 Wood, E. C., and Charest, J. R.: Chemical Amplification - Cavity Attenuated Phase Shift Spectroscopy Measurements of Atmospheric Peroxy Radicals, *Analytical chemistry*, 86, 10266-10273, 10.1021/ac502451m, 2014.
- Yang, M., Beale, R., Liss, P., Johnson, M., Blomquist, B., and Nightingale, P.: Air-sea fluxes of oxygenated volatile organic compounds across the Atlantic Ocean, *Atmos. Chem. Phys.*, 14, 7499-7517, 10.5194/acp-14-7499-2014, 2014.
- 1015 Zellweger, C., Steinbacher, M., and Buchmann, B.: Evaluation of new laser spectrometer techniques for in-situ carbon monoxide measurements, *Atmos. Meas. Tech.*, 5, 2555-2567, 10.5194/amt-5-2555-2012, 2012.
- 1020 Zellweger, C., Emmenegger, L., Firdaus, M., Hatakka, J., Heimann, M., Kozlova, E., Spain, T. G., Steinbacher, M., van der Schoot, M. V., and Buchmann, B.: Assessment of recent advances in measurement techniques for atmospheric carbon dioxide and methane observations, *Atmos. Meas. Tech.*, 9, 4737-4757, 10.5194/amt-9-4737-2016, 2016.